Single-Cell Transcriptomic Atlas Uncovers the Crucial Role of Monocyte-Derived CXCL10 and Identifies Viremia Biomarkers with Viral Genome Evolution during CHIKV Infection

Hongyang Yi[1*†], Zhenyu Yang[1*], Ruixue Dong[2*], Sumei Yang[1*], Xiaofu Wan[1], Feng Ouyang[2], Xiang Liu[1], Ying Tan[1], Shuhong Han[1], Yuanlong Lin[1], Weilong Liu[1], Tetsuya Asakawa[1], Jing Yuan[1], Mingxia Zhang[1†], Xiaohe Li[1†], Jiayin Shen[1†], Hongzhou Lu[1†]

[1]Institute for Hepatology, National Clinical Research Centre for Infectious Diseases, The Third People's Hospital of Shenzhen and The Second Affiliated Hospital of Southern University of Science and Technology, Shenzhen 518112, China.

[2]School of Life and Health Sciences, Hainan Province Key Laboratory of One Health, Collaborative Innovation Center of Life and Health, Hainan University, Haikou, Hainan 570228, China

[*]These authors contributed equally to this work.

[†]**Correspondence:**

Hongyang Yi: yihy2018@mail.sustech.edu.cn;

Mingxia Zhang: zmxmby@outlook.com;

Xiaohe Li: 13823526646@139.com;

Jiayin Shen: johnnie1111@163.com;

Hongzhou Lu: luhongzhou@fudan.edu.cn.

Graphical abstract

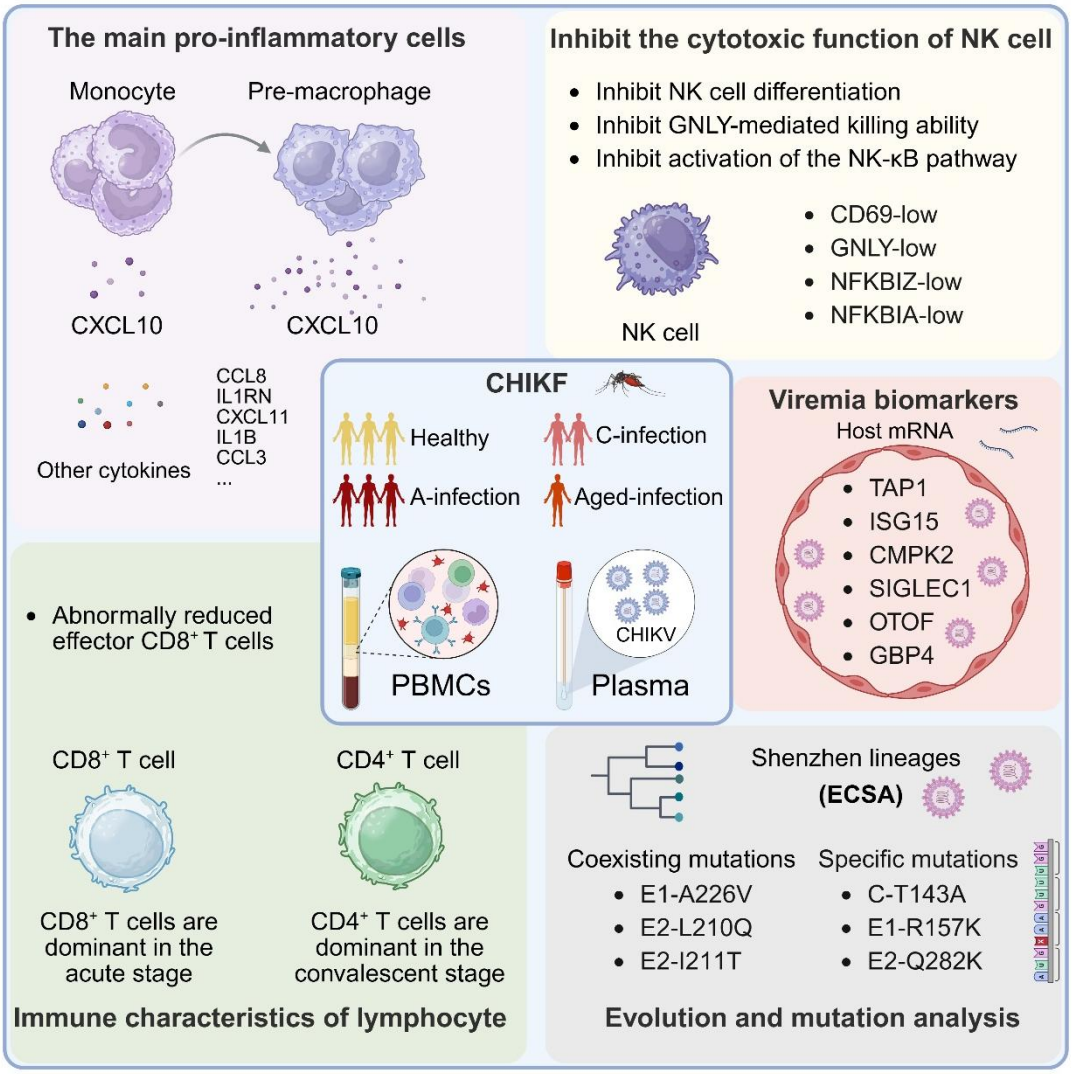

Highlights

- CXCL10, which is transcriptionally driven by pre-macrophages and monocytes, exerts a crucial role in the innate immune response during CHIKV infection.
- CHIKV induces elevated proportions of naive $CD4^+$ T and $CD8^+$ T cells, with $CD8^+$ T cell proportions declining during convalescence while $CD4^+$ T cell proportions remain persistently elevated.
- The interferon pathway is activated in all PBMCs and plays a key role in inhibiting viral replication, while the differentiation, killing and NF-κB pathway function of NK cells were inhibited.

- Plasma mRNA levels of TAP1, ISG15, CMPK2, GBP4, OTOF and SIGLEC1, along with CXCL10 cytokine, were identified as biomarkers associated with the severity of CHIKV viremia.
- Two genomically distinct CHIKV strains (ECSA) were identified, which harbor key mutations of E1-A226V, E2-L210Q and E2-I211T, besides specific mutations of C-T143A, E1-R157K and E2-Q282K.

Abstract

Widespread local transmission of Chikungunya virus (CHIKV) in China poses a severe challenge to public health. However, to date, the immunological characteristics of peripheral blood mononuclear cells (PBMCs) in CHIKV-infected individuals have not been characterized in a systematic manner, and specific plasma biomarkers for clinical diagnosis remain lacking. Herein, we applied single-cell RNA sequencing (scRNA-seq) to construct a high-resolution transcriptomic landscape of PBMCs from CHIKV-infected individuals for the first time. In combination with a 120-plex plasma cytokine assay and next-generation sequencing (NGS) of plasma RNA, we multi-dimensionally characterized the immunological features of CHIKV-infected patients and identified potential plasma biomarkers. Our analyses unveiled extensive activation of innate immune pathways marked by significant upregulation of interferon (IFN)-related signaling pathways in CHIKV-infected individuals. Notably, we identified CXCL10, a factor transcriptionally dominated by monocytes and pre-macrophage subsets, as a potential key immune mediator, and found that plasma host mRNAs including TAP1 and CMPK2, etc., could serve as potential auxiliary biomarkers for clinical diagnosis. Phylogenetic analysis demonstrated that the CHIKV strain circulating in Shenzhen belongs to the East/Central/South African (ECSA) genotype and harbors specific mutations of C-T143A, E2-Q282K and E1-R157K. Collectively, this study systematically depicts the peripheral blood immune responses of CHIKV patients from the perspectives of single-cell transcriptome, plasma host transcriptome and cytokines, providing valuable insights into the immunopathogenesis of CHIKV infection, the development of diagnostic biomarkers and the design of targeted therapeutic strategies.

Keywords: scRNA-seq; CHIKV; PBMCs; Pre-macrophage; CXCL10; ECSA; Cytokines.

Introduction

Chikungunya fever (CHIKF) is an acute mosquito-borne infectious disease caused by the CHIKV, characterized by high infectivity and rapid spread[1]. In recent years, the virus has become endemic in over 100 countries spanning Africa, the Americas, and Asia, with cumulative reported cases exceeding ten million and approximately 2.8 billion people at risk of infection, posing ongoing pressures on local public health and socioeconomic systems[2]. Of particular concern is that imported cases in Guangdong Province, China, have already triggered local transmission chains and show a potential trend of spreading to neighboring provinces[3]. Currently, there are no specific antiviral drugs globally targeting the CHIKV, nor any widely approved vaccines. Although the Ixchiq vaccine received approval from the US Food and Drug Administration (FDA) in 2023, its long-term protective efficacy and immune durability still require further validation in real-world settings[4]. Against this backdrop, elucidating the immunopathological mechanisms of the CHIKV have become critical challenges in the global public health domain.

The accelerated spread of the epidemic is fundamentally driven by the synergistic effects of viral evolution and environmental factors. Over the past few decades, *Aedes albopictus*, originally from Asia with a preference for animal blood-feeding, has gradually replaced *Aedes aegypti* as the primary vector for the CHIKV[5]. A key mechanism underlying this vector shift is the amino acid substitution at position 226 of the CHIKV E1 protein, where alanine is replaced by valine (E1-A226V)[6]. Studies have shown that, compared with *Aedes aegypti, Aedes albopictus* exhibits stronger ecological adaptability, with a distribution range extending into higher-latitude temperate regions and a higher susceptibility to the CHIKV, thereby significantly enhancing the transmission potential of the virus[7]. Concurrently, the virus itself has undergone adaptive evolution under the selective pressure of *Aedes albopictus*[8]. For instance, the E2-L210Q mutation further improves the transmission capacity and adaptability of CHIKV[9], while the E2-I211T mutation can partially relieve the epistatic

suppression effect on the E1-A226V mutation[10]. Phylogenetic analyses reveal that the CHIKV can be divided into four major geographic lineages: the West African, East-Central-South African (ECSA), ECSA-diverged or Indian Ocean Lineage (IOL) and Asian lineage[11]. The strains that have sporadically appeared in China previously mostly belong to the Asian type or the IOL type[12].

In terms of clinical manifestations, patients often present with acute fever, rash, and symmetric severe polyarthralgia, typically affecting the wrists, ankles, and knees. Notably, approximately 50% of infected individuals may develop chronic arthritis, with symptoms persisting for several years, severely impacting their quality of life and socioeconomic functioning[13]. Research shows that the CHIKV, has a short incubation period, and the acute phase is characterized by high-level viremia. During this stage, monocytes are extensively recruited to the sites of infection, differentiating into macrophages and releasing large quantities of pro-inflammatory factors. Meanwhile, activated T cells - particularly $CD4^+$ and $CD8^+$ subsets - participate in viral clearance and tissue damage through effector secretion and cytotoxic activities[14]. At the molecular level, type I and type II interferon pathways are rapidly activated, inducing the expression of hundreds of interferon-stimulated genes (ISGs) and establishing a broad antiviral state[15]. Simultaneously, key signaling pathways such as NF-κB are triggered by viral RNA, promoting the release of pro-inflammatory cytokines like IL-1β, IL-6, and TNF-α, as well as chemokines such as MCP-1 and CXCL10[16,17]. Notably, previous studies have indicated that the severity of CHIKV disease is closely associated with high serum levels of chemokines such as CXCL10[18]. These mediators not only further recruit immune cells, forming inflammatory infiltrates, but also directly increase vascular permeability, cause tissue edema, and induce pain sensitization, thereby collectively mediating the acute-phase rash and severe arthralgia, while also laying the foundation for the pathological progression of chronic arthritis[19].

Although previous studies have preliminarily uncovered the immunopathological features of CHIKF, a systematic understanding of the dynamic changes in peripheral immune cells throughout the entire disease course remains to be elucidated. Specifically,

the quantitative distribution, phenotypic characteristics, subset composition, and functional states of key immune populations, such as T cells, B cells, monocytes, and NK cells - across different disease stages have not been clearly defined. While conventional bulk RNA sequencing has provided valuable insights into systemic immune responses, its technical limitation in resolving cellular heterogeneity obscures critical cell type-specific information[20]. This methodological bottleneck is particularly pronounced in CHIKV research, as the differential responses of immune cell subsets are key determinants of viral clearance efficiency, disease progression trajectory, and the development of chronic joint symptoms. To overcome this limitation, we performed scRNA-seq analysis on peripheral blood mononuclear cells (PBMCs) from a well-defined clinical cohort. The cohort design included healthy controls, patients with acute - and convalescent-stage CHIKF, and a specifically incorporated older individual at higher risk of severe disease. Through this strategy, we achieved an unbiased dissection of the immune landscape during infection at single-cell resolution, precisely identifying various cell subsets, systematically characterizing their transcriptional dynamics across disease stages and age groups and thereby revealing the dysregulated cell type-specific signaling networks in CHIKV infection. To further validate these transcriptomic findings at the protein level, we employed high-throughput multiplex cytokine assays to quantitatively profile 120 key inflammatory mediators and chemokines in plasma. This approach not only provided proteomic corroboration of the scRNA-seq data but also uncovered functional insights at the post-transcriptional regulatory level. Leveraging its high sensitivity and multi-parameter simultaneous analysis capabilities, we were able to construct a comprehensive regulatory axis from gene expression to protein secretion, offering multi-dimensional experimental evidence for understanding the immune response mechanisms in CHIKF.

In summary, this study integrated single-cell transcriptomics, plasma proteomics, and viral evolutionary analysis to construct a framework of the host immune responses and genetic evolution of the CHIKV. We systematically characterized viral lineage features and simultaneously deciphered the specific immune cell and molecular events

triggered by infection, thereby revealing potential coupling relationships between viral variation and clinical immunophenotypes. This work establishes a multi-omics theoretical foundation for future precision prevention and treatment strategies.

Results

The scRNA-seq atlas of PBMCs from CHIKV-infected patients and healthy donors

To comprehensively characterize the peripheral immune response to CHIKV infection, we performed scRNA-seq on PBMCs isolated from 6 samples with CHIKV infection, including 3 acute-phase infection (A-infection), 2 convalescent-phase infection (C-infection) and 1 elderly A-infection, as well as 3 healthy donors **(Fig 1a)**, and also performed multi-cytokine detection and RNA sequencing for the patients' plasma. The demographics and clinical features of the patient cohort and healthy donors are summarized in **Table 1**. Samples were collected from patients at 3 to 8 days post symptom onset. Notably, lymphocyte counts in all patients were below the normal reference range. This observation may be attributable to direct viral invasion and destruction of lymphocytes, or alternatively, the massive mobilization of lymphocytes to infected sites (e.g., the ankle joint, rash area) for participation in local immune responses. Following stringent quality control **(Fig S1a)**, we obtained transcriptome data for a total of 81296 high-quality cells. Unsupervised clustering analysis identified 12 distinct cell clusters, which were visualized using t-distributed stochastic neighbor embedding (t-SNE) **(Fig 1b, Fig S1b)**. Each cluster was annotated according to well-established lineage-specific marker genes **(Fig 1c-d)**. Cluster 1 ($CD3D^+/CD3E^+/CD3G^+$) was identified as $CD4^+$ T cells, and Cluster 2 ($LEF1^+/TCF7^+/CCR7^+$) was annotated as naive $CD4^+$ T cells. Cluster 3, characterized by expression of CD8A, CD8B, CD3D, CD3E, and CD3G, was defined as $CD8^+$ T cells. Cluster 4, which also expressed CCR7, LEF1, and TCF7, was classified as naive $CD8^+$ T cells. Cluster 5, expressing MS4A1, CD79A, and CD79B, was identified as B cells. Cluster 6 (plasma B cells) exhibited high expression of JCHAIN, IGHG1, and IGHG2. Cluster 7 (monocytes) was marked

by VCAN, CD14, S100A8, and S100A9. Notably, we defined a cell cluster (Cluster 8) by its high co-expression of defining monocyte/macrophage markers (CSF1R, FCGR3A/CD16, CX3CR1, FCGR1A/CD64, CCR2). The combined evidence from its distinct transcriptomic signature and trajectory inference, which localized it to an intermediate state between monocytes and macrophages, provided compelling evidence to annotate it as "Pre-macrophage"[21-23]. Cluster 9 was annotated as conventional dendritic cells (cDCs) based on expression of CD1C, FCER1A, and CLEC10A. Cluster 10 was classified as plasmacytoid dendritic cells (pDCs) according to expression of LILRA4, FCER1A, and IRF7. Cluster 11, expressing KLRF1, NCAM1, and NCR1, was identified as NK cells. A small platelet population (Cluster 12) was defined by PPBP, PF4, and GP9 expression. These well-defined subsets were subsequently used to investigate cell-type-specific antiviral responses and immune dysregulation during CHIKV infection.

scRNA-seq reveals immune perturbations in acute CHIKV infection

Given that the acute phase of CHIKV infection represents a critical window for virus-host immune interaction, where cellular states closely resemble the "primary response" post-viral infection and can clearly reflect immune cell changes directly induced by the virus. However, the specific roles of viral replication and host immune responses in CHIKV infection have not been fully elucidated. Therefore, this study focused on dissecting the immunological characteristics of PBMCs during the acute infection phase using scRNA-seq. To characterize the functional states and dynamic changes of different cell populations in PBMCs from CHIKV-infected patients, we first performed tSNE dimensionality reduction analysis on PBMCs from the A-infection group and the normal group (control). The results showed that the proportions of monocytes, pre-macrophages, naive $CD4^+$ T cells, and naive $CD8^+$ T cells were increased in patients with acute infection, whereas the proportions of NK cells, $CD8^+$ T cells, and platelets were markedly decreased **(Fig 2a-b & Fig S2a)**. These findings indicate that innate and adaptive immune responses exert complex regulatory effects during the acute phase of CHIKV infection.

Subsequently, we analyzed the transcriptomic data of 12 cell populations and found that monocytes and pre-macrophages had the largest number of differentially expressed genes (DEGs). Additionally, many interferon-induced protein (IFIT) genes were significantly upregulated across all cell populations **(Fig 2c-d)**. Further Gene Ontology (GO) enrichment analysis of all cells revealed that the "*regulation type interferon production*" pathway was significantly activated, suggesting a crucial role of the interferon pathway in responding to acute CHIKV infection, which is consistent with previous studies[24]. Besides, pathways related to innate immune response, lymphocyte activation, and negative regulation of viral replication were also activated, indicating that the host is actively responding to exogenous viral invasion, although the underlying mechanisms require further investigation **(Fig 2d)**. In contrast, pathways such as ribosome biogenesis, translation, and nucleocytoplasmic transport were significantly suppressed in the acute stage of CHIKV infection **(Fig S2b)**. This may be attributed to the fact that viral genome replication and protein synthesis rely on the host's ribosomal and translational systems. The host cells limit the replication and spread of the virus within immune cells at the cost of "sacrificing part of their own protein synthesis".

The innate immune system serves as the first line of defense against CHIKV infection, with core functions including early viral recognition, initiation of rapid antiviral responses, restriction of viral replication and dissemination, as well as bridging the adaptive immune response - processes that are critical for controlling acute infection and preventing chronic pathological damage. Among innate immune mediators, type I interferons are central effector molecules in counteracting CHIKV infection[25]. To further evaluate the significance of interferon and inflammatory immune responses during CHIKV infection, we analyzed the expression levels of key innate immune pathways (defined by GO biological process terms) in the A-infection group. The results demonstrated that acute inflammatory responses, TNFα and TNFβ response, type I interferon responses, and type II interferon responses were significantly upregulated in most cell clusters, with particularly pronounced elevation in monocytes

and pre-macrophages **(Fig 2e & Fig S2c)**. This suggests that monocytes and pre-macrophages may act as crucial sources of innate immunity and inflammatory storms during the acute phase of CHIKV infection. In contrast, type III interferon responses showed no obvious overall activation and were even slightly downregulated in some cell clusters **(Fig S2c)**. IFN-α/β can bind to interferon receptors (IFNAR1/2) on the surface of host cells, thereby activating the JAK-STAT signaling pathway and inducing the expression of hundreds of interferon-stimulated genes (ISGs)[26]. To further confirm the critical role of the interferon pathway in CHIKV infection, we assessed the expression levels of ISGs in key cell clusters. The results showed that ISGs expression was significantly upregulated across all cell clusters, with the most striking increase observed in monocytes and pre-macrophages **(Fig 2f)**. These data further validate the central role of these two cell populations in mediating innate immune responses during the acute stage of CHIKV infection.

Dysregulated intercellular communication is a critical driver of exacerbated inflammation and tissue damage during viral infections. Therefore, we utilized CellChat to analyze 70 pivotal signaling pathways, with a focus on identifying cell populations that act as major senders (outgoing signaling) or receivers (incoming signaling) of intercellular cues. Following CHIKV infection, pre-macrophages and dendritic cells emerged as central hubs in the intercellular communication network, functioning as both predominant outgoing and incoming signaling cell populations. This dual role highlights their core position in coordinating immune responses during CHIKV infection. Post-infection, the outgoing signals of multiple pathways were significantly enhanced, including CALECTIN, PECAM2, ANNEXIN, LAIR1, TNF, CXCL (predominantly derived from pre-macrophages), CCL, TRAIL, and SN pathways. Notably, $CD8^+$ T cells in the infected group secreted CD69 signals - this may be a compensatory activation response of $CD8^+$ T cells to viral infection, despite their impaired proliferation and differentiation, reflecting an attempt to maintain partial immune surveillance function. In monocytes and pre-macrophages, the major incoming signaling pathways post-infection included CALECTIN, LAIR1, TRAIL, CCL, TNF,

and ANNEXIN, which may be involved in activating these cells to initiate antiviral responses. For NK cells, the key incoming signaling pathways were SN, PECAM2, VISFATIN, ADGRG, and NCAM, which may regulate NK cell activation, cytotoxicity, or differentiation during CHIKV infection **(Fig 2g-h & Fig S2c)**.

These results collectively confirm the crucial role of type I and type II interferon responses during acute CHIKV infection, as well as the roles of monocytes/pre-macrophages as key sources of innate immunity and hubs of intercellular communication, and initially clarify the immunological characteristics of acute CHIKV infection.

CXCL10 exerts a crucial role in monocytes and pre-macrophages during acute infection

Our findings demonstrated a significant increase in the proportions of monocytes (31.5%) and pre-macrophages (10.7%) in the acute phase of CHIKV infection, compared to the normal group (22.3% for monocytes and 2.4% for pre-macrophages, respectively). Notably, the proportion of pre-macrophages exhibited an exceptionally abnormal elevation, reaching a 4.5-fold increase **(Fig 2a-b)**. This observation suggests that these two cell populations play crucial roles in CHIKV immunity. Previous studies have indicated that monocytes and macrophages are more susceptible to CHIKV infection and serve as the primary infiltrating cell types at the infection site[27].

To dissect the specific immune responses of monocytes and pre-macrophages during the acute stage of CHIKV infection, we performed sub-clustering analysis on these two cell populations. Based on their gene expression patterns, they were categorized into 6 major subclusters **(Fig 3a)**. We observed that the proportions of Cluster 1, 2 and 5 were significantly reduced in the A-infection group, while the proportions of Cluster 3, 4 and 6 were markedly increased **(Fig 3b)**. Among these subclusters, Cluster 3 was primarily composed of pre-macrophages and showed the most prominent increase in proportion **(Fig 3c)**. Genes highly expressed in Cluster 3 included FCGR3A, HES4, SETBP1, and CDKN1C. Among these, FCGR3A mediates the phagocytic capacity of monocytes/macrophages and antibody-dependent cell-

mediated cytotoxicity (ADCC), thereby enhancing the ability to eliminate virus-infected target cells[28]. Subsequently, we analyzed the A-infection group at the transcriptomic level and found that CHIKV infection induced dramatic changes in the transcriptomic landscapes of monocytes and pre-macrophages **(Fig S3a, S3d)**. KEGG enrichment analysis demonstrated that the NOD-like receptor signaling pathway and Toll-like receptor signaling pathway were preferentially activated in both cell populations **(Fig S3b, S3e)**. This indicates that monocytes and pre-macrophages actively respond to viral invasion and serve a critical function in resisting CHIKV infection and regulating inflammation. Interestingly, we detected a significant upregulation in the transcriptional levels of the pro-inflammatory cytokine CXCL10 in both cell populations **(Fig S3a, S3d)**, suggesting that CXCL10 may act as a key mediator in viral immunity and inflammatory responses during infection. Therefore, we further analyzed the specific expression of CXCL10 across the 6 cell clusters. The results showed that the proportion of cells with high CXCL10 expression increased most significantly in Cluster 3 (pre-macrophages) of A-infection group **(Fig 3e)**. To further elucidate the role of CXCL10 in combating CHIKV infection, we isolated cell populations with high CXCL10 expression from monocytes and pre-macrophages in the A-infection group and compared them with those with low CXCL10 expression **(Fig S3g-S3h)**. Enrichment analysis of DEGs revealed that cells with high CXCL10 expression responded more actively to CHIKV infection, as pathways such as "*defense response to virus*" and "*regulation of innate immune response*" were preferentially activated. This further confirms the pivotal function of CXCL10 in CHIKV immunity.

To investigate the differentiation trajectory between different subsets of monocytes and pre-macrophages during the acute stage of CHIKV infection, we performed pseudotime analysis using Monocle2 and generated pseudotime trajectory plots to determine the relationship between cell differentiation trajectories and disease states. The analysis revealed that CHIKV infection promotes the differentiation of monocytes into pre-macrophages (Cluster 3) **(Fig 3h-i)**. We mapped the CXCL10-high cell population onto the trajectory plot and found that CXCL10-high cells were mostly

located at the terminal differentiation position, which largely corresponded to Cluster 3 (pre-macrophages) **(Fig 3j)**. This indicates that the CXCL10-high cell population is likely crucial in responding to CHIKV infection, and may play an essential role in promoting the conversion of monocytes to pre-macrophages, or facilitating the migration of pre-macrophages to infection sites and exerting immune functions at local infection foci.

To further explore the differentiation characteristics of monocytes and pre-macrophages in CHIKV-infected patients, we constructed a gene expression heatmap based on the pseudotime trajectory. Genes were categorized into two clusters according to the pseudotime trajectory: Cluster 1 represented genes upregulated in the late differentiation stage, while Cluster 2 represented genes downregulated in the late differentiation stage **(Fig 3k)**. Functional annotation of Cluster 1-related genes showed that many of these genes are directly or indirectly associated with the migratory capacity of monocytes/macrophages. For example, the Sell gene encodes L-selectin, which mediates the rolling adhesion of monocytes to vascular endothelial cells and serves as a critical initial step in migration[29]. CD53, a tetraspanin protein, regulates immune cell adhesion and migration[30]. SLAMF7 is upregulated following macrophage activation and enhances cell migration and infiltration[31,32]. Prostaglandins synthesized by PTGS2 (cyclooxygenase-2) act as important chemotactic signals for macrophage migration[33]. Both JUN (a member of the AP-1 family) and ATF3 are transcription factors that directly regulate the expression of migration-related genes (e.g., adhesion molecules and chemokine receptors)[34,35] **(Fig 3k & Fig S3k-o)**. Collectively, these results indicate that CHIKV infection induces the differentiation of monocytes into pre-macrophages and their subsequent infiltration into the infection site, whereby CXCL10 may act as a key mediator in this process.

Immune characterization of NK and CD8$^+$ T cells during the acute infection

In the acute stage of CHIKV infection, distinct from monocytes and pre-macrophages, the proportions of NK cells (6.6%) and CD8$^+$ T cells (11.4%) were significantly decreased compared to the normal group (17% for NK cells and 24.3% for

353 $CD8^+$ T cells, respectively) **(Fig 2a-b)**. This abnormal phenomenon may be closely
354 associated with immune dysfunction following CHIKV infection. Although NK cell-
355 mediated innate immunity and $CD8^+$ T cell-mediated adaptive immunity play important
356 part in CHIKV infection[36], the functional impacts of these cells on the progression of
357 CHIKV disease remain unclear. Given this, we conducted a detailed analysis of the
358 immunological characteristics of NK cells and $CD8^+$ T cells post-infection.

359 NK cells are present in the inflammatory microenvironment of many viral
360 infections, including CHIKV, and are among the earliest effector cells to respond to
361 viral invasion. They exert their functions by producing interferon-γ (IFN-γ), secreting
362 cytokines, and exerting cytotoxic effects[37]. Despite this, their function during CHIKV
363 infection remains undefined. Previous studies have suggested that NK cells can control
364 viral infection through specific expansion during the acute phase of CHIKV infection[38],
365 but our results showed the opposite trend. To address this discrepancy, we performed
366 sub-clustering analysis on NK cells, which were classified into 3 major subclusters
367 based on gene expression patterns: Cluster 1 consisted of naive NK cells, while Clusters
368 2 and 3 belonged to effector NK cells. The results revealed a significant increase in the
369 proportion of naive NK cells in the A-infection group **(Fig 4a-b)**, implying that the
370 differentiation and proliferation capacities of NK cells may be affected by CHIKV
371 infection. We further used CytoTRACE to evaluate the differentiation potential of
372 different single-cell subclusters. As shown in **Fig 4c and Fig S4a**, Clusters 1, 2, and 3
373 in the infection group exhibited higher CytoTRACE scores than those in the normal
374 group - an indicator of superior differentiation potential. This finding further confirms
375 that CHIKV infection can inhibit the proliferation and differentiation of NK cells. DEG
376 analysis of terminally differentiated infected NK cell Cluster 3 identified significant
377 enrichment of viral defense-related terms **(Fig 4d & S4b-c)**. To better construct the
378 differentiation trajectory of NK cells and clarify their dynamic changes during
379 development, differentiation, or CHIKV infection, we performed pseudotime analysis
380 on NK cells from the normal group and A-infection group. The results showed that,
381 compared to the differentiation trajectory of NK cells in the normal group (fate2), NK

cells in the A-infection group differentiated in the opposite direction (fate1) (**Fig 4e-f**). This indicates that although NK cells from both the normal and A-infection groups can be divided into three similar subclusters, the gene expression patterns of NK cells have undergone fundamental changes post-infection. Specifically, the fate of NK cells underwent a programmed shift at the Branch3 decision point (**Fig 4e-f**). We therefore analyzed the Branch3 fate decision point and found that fate1-related genes were closely associated with the inhibition of viral replication (**Fig 4g-h**). This suggests that NK cells initiate an innate immune response against the virus in the acute stage of CHIKV infection, which is consistent with relevant reports[37]. Notably, fate2-related genes were enriched in pathways such as "*response to tumor necrosis factor (TNF)*" **(Fig 4i)**, indicating that the TNF-mediated innate immune pathway of NK cells is inhibited in the acute stage of CHIKV infection-a striking observation. In addition, the upregulation of genes such as CD69 (a marker of NK cell activation) and GNLY (a marker of NK cell effector function) in fate2 implies that the partial activation status and cytotoxic function of NK cells are suppressed in the A-infection group **(Fig 4j)**. In summary, these results demonstrate that although NK cells play an important role in antiviral immunity following CHIKV infection, the CHIKV virus can partially inhibit the differentiation of NK cells into effector cells and impair some of their functions - such as suppressing the activation of the TNF pathway in NK cells.

A previous study reported that lymphopenia was a major laboratory feature in patients with acute chikungunya fever during the Reunion Island outbreak[39]. Our research further confirmed that the reduced lymphocytes are primarily $CD8^+$ T lymphocytes. However, the role of $CD8^+$ T cells in the pathogenesis of CHIKV remains poorly understood. Our results showed that although the overall proportion of $CD8^+$ T cells was significantly downregulated post-infection, the proportion of naive $CD8^+$ T cells in the A-infection group (7.1%) was indeed upregulated compared to the normal group (4.9%) **(Fig 2a-b)**. Based on gene expression patterns, $CD8^+$ T cells (including naive $CD8^+$ T cells) were classified into 6 major subclusters, with Cluster 1 identified as naive $CD8^+$ T cells and its proportion increased 2.3-fold after infection **(Fig 4k-i &**

S4d-e). DEG analysis revealed that Naive $CD8^+$ T cells (C1) in the A-infection group had already initiated a robust immune response to CHIKV infection **(Fig S4f-h)**. Pseudotime analysis revealed that the proportion of cells at early pseudotime stages in the A-infection group was significantly increased compared with the normal group regarding cellular differentiation trajectories **(Fig 4m-n)**. Subsequently, we constructed a pseudotime trajectory heatmap based on gene expression patterns. Genes associated with Cluster 2 were significantly upregulated at late pseudotime stages, and enrichment analysis identified significant enrichment of immune activation-related terms **(Fig 4p)**. In contrast, genes related to Cluster 1 were markedly upregulated at early pseudotime stages, and enrichment analysis of these genes showed enrichment for both cytoplasmic translation and ribosomal biogenesis terms **(Fig 4q)**. CytoTRACE analysis was performed to assess the differentiation potential of distinct subsets in the A-infection and normal groups, which revealed that the differentiation potential of $CD8^+$ T cells was not inhibited by CHIKV infection **(Fig S4i)**. This finding suggests that the abnormally increased naive $CD8^+$ T cells may result from elevated emergency thymic output or proliferation of the peripheral resting naive pool. Interestingly, we found that KLF7 - a gene highly expressed at the early stage of pseudotime that promotes the survival and proliferation of naive T cells - was conversely downregulated in the A-infection group **(Fig S4j)**, implying that CHIKV infection does not enhance the survival and proliferation of naive T cells. Subsequently, we annotated naive $CD8^+$ T cells (C1) using the marker panel for newly thymus-emigrated cells ($PECAM1^+PTPRC^+CCR7^+$), and found that the expression of this marker panel was rather lower in the A-infection group **(Fig S4k)**, which indicates impaired thymic output capacity. Therefore, the abnormal increase in naive $CD8^+$ T cells following CHIKV infection remains unexplainable based on the current experimental evidence. In summary, we confirmed that CHIKV acute infection-induced lymphopenia is primarily attributable to the reduction in $CD8^+$ T lymphocytes, while the proportion of naive $CD8^+$ T lymphocytes is significantly elevated, and the underlying mechanism requires further investigation.

Elevated plasma CXCL10 drives innate-adaptive immune crosstalk during CHIKV infection

After comprehensively delineating the intricate heterogeneity of immune cells and dynamic transcriptional programs at single-cell resolution, we sought to further determine whether these cell-intrinsic alterations are reflected in the systemic circulation - a critical link between local immune responses and systemic pathophysiological changes during infection. To address this pivotal question, we systematically profiled the plasma concentrations of 120 functionally relevant proteins via the high-sensitivity Human Cytokine Array Q2000 platform. The analysis was performed on clinical samples specifically collected from individuals during the acute phase of viral infection, ensuring the capture of initial immune activation events.

To facilitate a more systematic and hierarchical interpretation of the cytokine atlas, we categorized these 120 plasma factors into four functionally distinct groups based on their well-characterized biological roles: pro-inflammatory mediators, anti-inflammatory mediators, chemokines, and growth factors. Subsequent comparative analysis between the A-infected group and normal group revealed a widespread and prominent elevation in the plasma levels of most of the profiled factors in infected individuals **(Fig 5a-e)**. Specifically, 54 of these plasma factors met our predefined stringent significance criteria (FC > 2 and p.adj < 0.05) and were thus identified as significantly upregulated during the A-infection stage, reflecting a robust systemic immune activation **(Fig 5a)**. We then extended our analysis to explore the expression patterns of these 120 plasma-related factors in our previously generated scRNA-seq dataset **(Fig 5f)**. Applying the same stringent statistical criteria (FC > 2 and p.adj < 0.05), we identified a notable overlap between the plasma proteomic and single-cell transcriptomic profiles: 14 genes were consistently differentially expressed in both datasets. Notably, these 14 co-differentially expressed genes included several key immune regulators with well-established roles in infection and inflammation: CXCL10, CCL8, CXCL11, CCL7, AXL, IL1RN, IL1B, CCL20, IGF1, FGF7, CSF1, LIF, CCL3, and TIMP1 **(Fig 5g)**. Among these, multiple factors stand out for their conserved and

critical functions in viral infection: CXCL10 and CXCL11 (both the ligands of CXCR3) are potent chemoattractants for antiviral effector cells like T lymphocytes and NK cells, driving immune cell trafficking to infection foci[40]; CCL3, CCL7, and CCL8 recruit monocytes and neutrophils to amplify local innate immunity[41]; IL1B is a central pro-inflammatory cytokine that exacerbates antiviral immune responses and mediates infection-associated inflammation; and CSF1 promotes the differentiation and activation of macrophages-key cells for viral phagocytosis and antigen presentation[42]. Among these virus-relevant factors, CXCL10 emerges as the most prominently induced in our multi-omics data, warranting further exploration of its role and cellular source in acute viral infection **(Fig 5h)**. Importantly, our scRNA-seq data further pinpointed that monocyte/pre-macrophage, two key myeloid precursor subsets identified in our earlier single-cell analysis represented the predominant cellular source of CXCL10 and other important cytokines **(Fig 5i)**. This finding thereby establishes a clear cellular origin for the marked elevation of CXCL10 observed in the plasma of individuals with acute-stage infection. Previous studies have demonstrated that monocyte-derived macrophages migrate to the sites of infection in response to activation signals from chemokines such as CCL2 upon CHIKV induction[43]. Our findings, however, revealed that although CCL2 and its receptor CCR2 were both significantly highly expressed in monocytes, the pre-macrophages with high expression of both molecules accounted for a small proportion of the total population **(Fig S5a-b)**. This may be attributed to the fact that pre-macrophages highly expressing CCL2 and CCR2 had migrated to the infection sites to exert their functional roles, whereas the blood-resident pre-macrophages with low expression of these two molecules were incompletely differentiated or undertake other critical biological functions. We further performed ELISA validation for plasma CXCL10 levels in CHIKV-infected patients, which revealed that plasma CXCL10 expression was significantly elevated in all infected patients compared with the normal group **(Fig 5j)**. CXCL10 functions as a key IFN-inducible chemokine that specifically binds to its cognate receptor CXCR3, thereby regulating the migration and activation of effector immune cells (e.g., T cells and NK cells) and acting as a central “immune

497 regulatory hub" in various RNA and DNA viral infections[44]. However, our results
498 demonstrate that cell-cell communication between CXCL10-high expressing cells and
499 other PBMCs is restricted to pDCs **(Fig 5k-l)**, and the expression level of CXCR3 is
500 low in almost all PBMC populations except pDCs **(Fig 5m)**. This key phenomenon,
501 which is inconsistent with previous studies, suggests that CXCL10 may not be critical
502 in directly mediating immune cell migration during CHIKV infection. Instead, it may
503 act on other untested cell types to exert other important functions. Or there may be
504 undiscovered target receptors for CXCL10 in mediating immune cell migration, and
505 the underlying mechanisms warrant further investigation. We then analyzed the
506 transcription factors highly expressed in monocytes and pre-macrophages following
507 CHIKV infection and identified several key transcription factors, including ATF3, IRF7,
508 STAT1, STAT2 and others **(Fig S5c-d)**. Furthermore, CXCL10 exhibited a moderate
509 correlation in expression levels with the gene sets associated with these transcription
510 factors **(Fig S5e-j)**. WGCNA analysis revealed that the high expression of CXCL10 in
511 Module 2 **(Fig S5k-m)** - an expression module highly correlated with pre-macrophages
512 - was potentially associated with genes such as NFKBIZ, FCGR3A, CTSC and
513 CDKN1C **(Fig 5n)**.

514 In summary, during acute CHIKV infection, the potent and specific induction of
515 CXCL10 may serve as a key chemotactic and signaling hub. Its prominent function in
516 plasma cytokines suggests that CXCL10 could be used as a clinical biomarker.
517 However, the key molecular mechanisms by which it coordinates innate and adaptive
518 immune responses, or its role in promoting or inhibiting CHIKV replication, remain to
519 be explored.

520 **Convalescence-dependent immune features and age-associated impairment**

521 CHIKV infection induces severe symptoms in patients during the acute phase and
522 is often accompanied by persistent manifestations in the convalescent phase. Therefore,
523 it is essential to investigate the immunological characteristics of distinct PBMC subsets
524 and cytokines across different stages of CHIKV infection. Our results showed that
525 compared with the acute infection phase, the proportions of various cell subsets in

convalescent patients underwent significant dynamic changes: pre-Macrophages and monocytes exhibited a trend of first increasing (acute phase) and then decreasing (convalescent phase), while NK cells and $CD8^+$ T cells displayed the opposite pattern of first decreasing and then increasing. Notably, naive $CD4^+$ T cells, naive $CD8^+$ T cells, and total $CD4^+$ T cells maintained a continuous upward trend throughout the infection course, which may indicate that pre-Macrophages, monocytes, NK cells, and $CD8^+$ T cells may dominate the immune response during the acute phase of CHIKV infection, whereas $CD4^+$ T cells mediate adaptive immune responses in the later post-infection stages **(Fig 6a-b & S6a)**. The sustained elevation of naive $CD4^+$ and naive $CD8^+$ T cells is presumably driven by two main factors. First, CHIKV infection triggers the thymic emergency output of naive T cells, accelerating the differentiation and maturation of immature T cells that are subsequently massively released into the peripheral blood to replenish the immune pool. Second, it may result from the enhanced proliferative capacity of peripheral resting naive T cells. Additionally, compared with patients in the acute infection phase, those in the convalescent infection phase showed reduced acute inflammatory responses and interferon responses **(Fig 6c)**, which suggests that the body's robust pro-inflammatory state gradually subsides in the convalescent phase, and the immune system transitions from an acute anti-viral defense mode to a state focused on restoring immune homeostasis.

Subclustering analysis of key cell subsets further revealed stage-specific features: for pre-Macrophages and monocytes, the proportions of major subclusters (C1, C2, C3) were restored to a near-normal state in the convalescent phase **(Fig 6d-e)**, and terminally differentiated cells with high CXCL10 expression were also reduced compared with those in the acute phase of infection **(Fig 6f-g)**. Consistently, CXCL10-whose expression is pivotal in the acute phase - was rapidly downregulated at this stage, further confirming its pivotal role in acute CHIKV infection **(Fig 6h)**. Similarly, the expression levels of IL1RN and IL1B, which are highly upregulated in A-infection group, also decreased sharply in the convalescent phase **(Fig S6b)**. For NK cells, although the proportion of subcluster C3 continued to increase from the acute to the

555 convalescent infection phase (in contrast to the decreasing trend of C2), the
556 differentiation capacity of C1 and C2 subclusters was significantly restored in the
557 convalescent phase **(Fig 6j-l)**. For naive $CD8^+$ T cells and total $CD8^+$ T cells,
558 subclustering analysis showed a slight increase in the proportion of subcluster C1 (naive
559 $CD8^+$ T cells) in the convalescent infection phase, and except for subcluster C4, the
560 proportions of other subclusters either continued to rise or fall, implying that $CD8^+$ T
561 cell-mediated cellular immunity still plays an key function in the convalescent stage of
562 infection **(Fig 6m-n)**. Moreover, pseudotime analysis revealed that the proportion of
563 $CD8^+$ T cells at the early pseudotime stage in the convalescent phase tends to approach
564 an immune homeostasis state **(Fig 6o& S6c)**. Additionally, subclustering analysis of
565 $CD4^+$ T cell subsets showed that the proportion of naive $CD4^+$ T cells (Cluster 1)
566 slightly increased during the acute infection phase but markedly increased in the
567 convalescent phase **(Fig 6p-q & S6d)**. Pseudotime analysis further revealed that the
568 gene expression profiles of the massively increased naive $CD4^+$ T cells in the
569 convalescent phase appeared to be in the late pseudotime stage **(Fig 6r-s & S6e)**,
570 indicating that these cells may be in a transitional state between naive and antiviral
571 infection states and play an important role in antiviral immunity during the convalescent
572 phase.

573 Notably, we also included an elderly patient in our analysis and found that in the
574 acute infection phase, the elderly patient exhibited weaker acute immune responses and
575 interferon responses compared with young patients **(Fig S6f)**; furthermore, the
576 expression levels of CXCL10, IL1RN, and IL1B - key immune factors that exert crucial
577 anti-CHIKV effects - were significantly lower in the elderly patient than in young
578 patients **(Fig S6g)**. These findings suggest that the anti-infection immune response is
579 relatively impaired in elderly patients, which may be a key factor contributing to
580 potential differences in disease severity, clinical outcomes, or recovery rates between
581 elderly and young populations infected with CHIKV.

582 These results investigated immunological characteristics of PBMC subsets and
583 cytokines across CHIKV infection stages. Convalescent patients showed dynamic cell

proportion changes. Acute inflammatory/interferon responses subsided in convalescence, with restored subcluster proportions of key cells, downregulated CXCL10/IL1RN/IL1B, and recovered NK cell differentiation. Notably, elderly patients exhibited impaired immune and interferon responses with lower key factor expression.

Phylogenetic analysis of Shenzhen strains and identification of marker genes for viremia severity

Previous studies have demonstrated a high degree of homology between the Foshan CHIKV strain and the Réunion CHIKV strain, suggesting that the endemic Foshan CHIKV strain may have originated from Réunion. However, it remains unclear whether the local outbreak in Shenzhen is associated with the Foshan outbreak or represents an independent imported event. To address this uncertainty, we extracted RNA from the serum of patients at different infection stages for next-generation sequencing (NGS) to perform viral genetic analysis, and simultaneously detected the abundance and types of host mRNA in serum as potential “auxiliary markers” for the severity of viremia. Among the 5 enrolled patients, complete viral sequences were detected in 2 cases (viremic patients) with an admission time of 3 days post-onset, while no complete viral sequences were identified in the other 3 cases (convalescent patients) whose admission time was 4-8 days post-onset **(Fig 7a)**. These findings indicate that the time window of viremia following CHIKV infection occurs within 3 days post-onset. Notably, a substantial amount of host mRNA information was detected during the analysis of the viral genome in serum. To identify host serum markers indicative of viremia severity, we compared the serum mRNA profiles of the 2 viremic patients with those of the 3 convalescent patients (control group). The results showed that numerous host genes were highly expressed in the serum of infected patients, including *TAP1*, *ISG15*, *CMPK2*, *GBP4*, *OTOF*, and *SIGLEC1* **(Fig 7b)**. Further analysis revealed a strong positive correlation between the expression levels (FPKM values) of these genes in serum and the viral gene content (FPKM values) **(Fig 7c)**. We also validated the expression of these host genes in serum by qPCR, and the results similarly confirmed a high positive correlation between the expression of these host genes and viral gene

content (FPKM values) **(Fig 7d)**. These data suggest that these host genes in serum can serve as "auxiliary markers" for the severity of viremia. Subsequently, we measured the mRNA levels of these genes in the serum of healthy volunteers. Compared with infected patients, the expression of these 6 genes was barely detectable in the serum of healthy volunteers, which further confirms the reliability of these genes as markers for the severity of CHIKV viremia **(Fig 7e)**. Combined with single-cell sequencing data analysis, we found that genes with a strong correlation ($R^2 \geq 0.98$), such as *TAP1*, *ISG15*, *CMPK2*, and *GBP4*, were highly expressed in almost all PBMCs and were closely associated with the activation of the interferon pathway. In contrast, genes with a relatively weak correlation ($0.9 \leq R^2 < 0.98$) tended to be expressed in monocyte, pre-macrophage and cDC **(Fig 7f)**. Specifically, *SIGLEC1* is involved in the activation-driven process of macrophages[45], while *OTOF* is associated with calcium-dependent vesicle release[46]. Collectively, these results indicate that CHIKV infection elicits immune responses in almost all PBMC populations, and monocyte/pre-macrophages-related specific immune responses are also crucial. The aforementioned mRNAs can serve as "auxiliary markers" for the severity of viremia. We further performed IGV analysis to assess the integrity of these relevant genes in serum and found that all six genes had intact transcript structures **(Fig 7g & Fig S7a-d)**. This implies that host mRNA in serum is more likely derived from active cellular efflux rather than fragmented gene leakage caused by cell death.

Phylogenetic tree analysis showed that the Shenzhen CHIKV strain shared high homology with the East/Central/South African (ECSA) lineage strain (MT666071.1) and belonged to the ECSA lineage **(Fig 7h)**. This suggests that the endemic Shenzhen strain is most likely derived from imported cases rather than the previously sporadic strains circulating in China. Mutation analysis revealed that both the Shenzhen strain and MT666071.1 harbored the combined mutations of E1-A226V, E2-L210Q and E2-I211T, and these adaptive mutations enhance the transmission capacity of CHIKV. In addition, compared with MT666071.1, the Shenzhen strain also carried the C-T143A mutation (which enhances the transmission capacity of CHIKV in Aedes aegypti), the

E2-Q282 mutation, and the E1-R157K mutation **(Fig 7i)**. Whether the latter two mutations can promote CHIKV transmission remains unclear. These genetic characteristics help explain the rapid spread of the outbreak. Notably, a large number of nucleotide and amino acid mutations were also detected between the two Shenzhen strains, of which two codon mutations caused amino acid changes (NSP1-I468V, NSP3-V189A) **(Fig 7j)**.

In summary, the above study performed viral genetic analysis and plasma mRNA profiling to investigate the Shenzhen CHIKV outbreak and identify viremia-associated markers. Viral sequencing revealed viremia occurs within 3 days post-onset, and 6 host genes (e.g., TAP1, ISG15) in serum were validated as reliable auxiliary markers for viremia severity. Phylogenetic analysis showed the Shenzhen strain belongs to the ECSA lineage, likely imported rather than derived from domestic sporadic strains, and harbors multiple adaptive mutations (e.g., E1-A226V) enhancing transmission capacity, plus unique mutations. Notable genetic variations were also found between the two Shenzhen strains, indicating that CHIKV is undergoing rapid mutation during local transmission or that the two Shenzhen cases may originate from distinct infection sources.

Discussion

This study systematically delineates the immunopathological mechanisms and viral evolutionary characteristics of CHIKV infection through an integrated multi-omics approach, including scRNA-seq, plasma cytokine profiling, and NGS. By analyzing PBMCs and plasma samples from CHIKV-infected patients across different disease stages and age groups, we provide a comprehensive understanding of host-virus interactions, identify novel biomarkers, and clarify the genetic features of the circulating strain in Shenzhen **(Fig 8)**.

A key novelty of this work is the first comprehensive single-cell transcriptomic atlas of PBMCs from CHIKV-infected patients, spanning acute and convalescent infection stages and including elderly individuals, revealing the dynamic perturbations

of immune cell subsets. Consistent with previous transcriptomic studies[47,48], we observed robust activation of innate immune pathways, including IFN signaling and NF-κB-mediated pro-inflammatory responses. Monocytes and pre-macrophages are significantly expanded in the acute phase, serving as key sources of innate immunity and inflammatory mediators. Importantly, our single-cell data demonstrate that lymphopenia observed in blood routine blood tests **(Table 1)** is primarily attributed to the abnormal reduction of effector $CD8^+$ T cells **(Fig 4i)**. Thus, we postulate that lymphopenia in CHIKV-infected patients is most likely caused by the massive infiltration of effector $CD8^+$ T cells into infected tissues, a phenomenon previously reported in the literature[49]. Naturally, we cannot rule out the possibility that CHIKV may induce effector $CD8^+$ T cell exhaustion and death, though no evidence has been found to support this possibility to date. Notably, we also found that the proportion of NK cell populations in CHIKV-infected patients is abnormally decreased, and their differentiation capacity, partial cytotoxic function, and NF-κB pathway are partially suppressed. This is inconsistent with previous studies reporting the specific expansion of NK cell subsets during acute CHIKV infection[38]. Further verification is needed to determine whether this phenomenon is associated with differences in viral strains. We also characterize the stage-specific immune remodeling: the acute phase is dominated by robust interferon and pro-inflammatory responses, while the convalescent phase features a transition toward immune homeostasis, with sustained elevation of naive $CD4^+$ T cells mediating long-term adaptive immunity[50]. Additionally, elderly patients show impaired immune activation and reduced expression of key factors (e.g., CXCL10, IL1RN), suggesting age-related vulnerability that may influence clinical outcomes.

Furthermore, our multi-omics analyses and experimental validation further confirm that CXCL10 is a key immune mediator of CHIKV infection. Both scRNA-seq and high-throughput plasma cytokine analyses demonstrate that CXCL10 is mainly secreted by monocytes and pre-macrophages, which is significantly upregulated during the acute phase of infection and transitions toward homeostasis in the convalescent phase. CXCL10 may exert a double-edged sword role in antiviral immunity: our data

show that CXCL10-high expressing cells exhibit enhanced antiviral pathways (e.g., "defense response to virus"), while other studies have reported that CXCL10 signaling promotes the persistence of CHIKV[51] and HIV[52] in tissue-infiltrating macrophages. This discrepancy suggests that the function of CXCL10 is context-dependent (possibly associated with infection stage, cell type, or viral load), and further studies using in vitro and in vivo models are required to clarify whether it exerts a protective or pathogenic role.

In addition, NGS and plasma transcriptomic analyses identify six host mRNAs (TAP1, ISG15, CMPK2, GBP4, OTOF, SIGLEC1) as reliable auxiliary biomarkers for viremia severity, with intact transcripts indicating active cellular efflux rather than cell death-induced leakage. These biomarkers exhibit strong correlation with viral load and offer potential for early clinical diagnosis. Phylogenetic analysis further confirms that the Shenzhen CHIKV strain belongs to the ECSA lineage, harboring adaptive mutations (E1-A226V, E2-L210Q, E2-I211T) enhancing vector transmission and unique mutations (C-T143A, E1-R157K, E2-Q282K), providing insights into the outbreak's origin and rapid spread.

Despite these insights, several limitations should be acknowledged. First, the definition of "acute" and "convalescent" stage relies solely on the onset of clinical symptoms (e.g., rash appearance), as precise infection timepoints could not be traced. Given CHIKV's short incubation period[53], viral replication may initiate days before symptom manifestation, which may lead to misclassification of disease stages and confound interpretations of immune cell dynamics. Second, our analysis of age-related immune responses is based on a single elderly patient. Although we observed weaker interferon responses and lower expression of key immune mediators (e.g., CXCL10, IL1RN, IL1B) in this individual compared to younger patients, this finding lacks statistical power and cannot be generalized to the broader elderly population. Larger cohorts of elderly patients are therefore needed to confirm age-related immune impairments and their potential impacts on disease severity and clinical outcomes. Third, the mechanism underlying the expansion of naive $CD8^+$ T cells remain elusive.

While our data indicate enhanced proliferative capacity of these cells, we cannot distinguish between two potential drivers: increased thymic emergency output of naive T cells or enhanced proliferation of peripheral resting naive T cells. Future studies should incorporate thymic function assays (e.g., T cell receptor excision circle [TREC] analysis) to clarify this ambiguity. Finally, the molecular basis for CHIKV-mediated suppression of NK cell differentiation remains unknown. Although viral proteins such as NSP3 have been shown to inhibit NF-κB signaling[16], it remains unclear whether they directly target the differentiation pathways of NK cells or act indirectly via myeloid-derived suppressor factors - an area requiring further exploration.

Collectively, this study integrates scRNA-seq, plasma cytokine profiling and genomic data to unravel the complex immune networks and viral evolution during CHIKV infection. The findings advance our understanding of CHIKV immunopathogenesis, offer novel diagnostic biomarkers (e.g., plasma CXCL10 and host mRNAs), and identify potential therapeutic targets (e.g., CXCL10), laying a foundation for precision prevention and treatment of CHIKV infection.

Materials and methods

1. Ethics approval and participant consent

This research plan was approved by the Human Ethics Committee of The Third People's Hospital of Shenzhen and The Second Affiliated Hospital of Southern University of Science and Technology. The ethical number is No.2024-013-02.

2. scRNA-seq Data Processing and Analysis

2.1 scRNA-seq library construction and sequencing

scRNA-seq libraries were constructed using the Single-Cell Full-Length RNA Transcriptome Sequencing Kit (Catalog No. K00801-08; SeekGene Co., Ltd., Beijing, China). Libraries were then sequenced on the Illumina NovaSeq 6000 platform (Illumina, Inc., San Diego, CA, USA) using paired-end sequencing with a 150 bp read length (PE150).

2.2 Processing and Quality Control of scRNA-seq Data

Raw sequencing reads were processed through the Seeksoultools pipeline (v1.2.2) using default recommended parameters. FASTQ-formatted Illumina data were aligned to the GRCh38-2020-A reference genome with STAR (v2.7.10a). Following alignment, unique molecular identifiers (UMI) were counted and non-cell-associated barcodes were filtered out to construct a gene-barcode matrix for each sample, containing cell barcodes and corresponding gene expression counts. The resulting matrix was imported into the Seurat R package (v5.2.1) for quality control and downstream scRNA-seq analysis. Unless otherwise stated, all functions were executed with default parameters. Cells exhibiting a high proportion of mitochondrial genes expression or identified as doublets were filtered out. Quality control was carried out based on three standard metrics: the number of detected transcripts (UMI), the number of detected genes, and the percentage of reads mapped to mitochondrial genes (filtered using quartile-based thresholds). A subset of variable genes was then extracted from the normalized data,

with expression variability controlled relative to the mean using the NormalizeData function in Seurat.

2.3 Cell Clustering and Annotation

Graph-based clustering was performed on Principal Component Analysis (PCA)-reduced data using the shared nearest neighbor (SNN) graph and Louvain algorithm. For sub-clustering analyses, the same preprocessing pipeline-including scaling, dimensionality reduction, and clustering procedures-was applied to subset datasets, which were typically restricted to a single cell type. Seurat's FindClusters function was utilized for clustering of cell sub-clusters. Differential gene expression (DGE) analysis was conducted for each cluster using the Wilcoxon rank-sum test to identify significantly differentially expressed genes relative to all other clusters. Cell type annotation was performed using Single-Cell Integrative Annotation (SCINA), guided by established cell-type marker genes. Dimensionality reduction was performed using both PCA and uniform manifold approximation and projection (UMAP), facilitating data visualization and validation of clustering structures.

2.4 Differential Expression Analysis and Functional Enrichment

DGE analysis between healthy control and infected samples was performed at the single-cell level using Seurat's FindMarkers function. To identify cluster-enriched genes-genes with significantly higher expression in specific cell clusters relative to all other clusters-the following criteria were applied: (1) expressed in ≥40% of cells within the target cluster; (2) expressed in ≤20% of cells across all other clusters; (3) statistical significance (adjusted p-value ≤ 0.05); and (4) high expression change (log2FC≥ 0.5). The top three genes per cluster, ranked by log2FC in descending order, were selected as cluster-specific marker genes. Dot plots illustrating marker gene expression across clusters were generated using Seurat's DotPlot function, with adjustments for visualization clarity (e.g., optimized gene labeling, dot size scaling). The same DotPlot function-with the split.by parameter (e.g., set to "sample group" for cohort distinction)-was further used to visualize key gene expression patterns across fresh samples within

each cluster. Additionally, Seurat's AddModuleScore function was employed to calculate enrichment scores for a predefined target gene set (e.g., infection-related pathways). Cells with high correlation to this gene set were identified using quartile-based thresholds.

2.5 Pseudotime Analysis

Pseudotime trajectory inference was performed using the DDRTree algorithm in Monocle (v2.32.0). Log-normalized data from the Seurat object were imported into Monocle, and gene expression profiles were used to identify variable genes with cell-type-specific expression across cell groups and assess the statistical significance of these findings. Cells were ordered along the pseudotime trajectory and visualized in a reduced-dimensional space. To explore dynamic expression patterns, genes were grouped based on similar expression trends over pseudotime. Branch points in the trajectory were analyzed to identify genes associated with lineage divergence. Differential gene testing was applied to select genes significantly correlated with pseudotime progression or branch specification. Genes with significant branch-dependent expression were further visualized using the plot_genes_branched_heatmap function.

2.6 Analysis of Cell-Cell Communication

Intercellular communication networks among identified cell types were analyzed using the CellChat R package (v2.1.2). For each experimental condition, a separate CellChat object was created and subsequently merged into a unified object via the mergeCellChat function. Interaction counts and communication strengths were evaluated using compareInteractions. Differences in the number and intensity of cellular interactions between the two datasets were visualized as a heatmap generated by netVisual_heatmap. Signaling pathway relatedness was quantified using the rankSimilarity function. The netAnalysis_signalingRole_scatter function was applied to identify significant changes in signaling sending and receiving roles across cell types. Specific alterations in signaling within selected cell populations were further investigated using

825 netAnalysis_signalingChanges_scatter. Finally, communication patterns of individual
826 signaling pathways were compared across conditions using the netVisual_aggregate
827 function.

828 **2.7 Transcription Factor Regulon Analysis**

829 Transcription factor (TF) regulatory networks and regulon activities were characterized
830 using the pySCENIC toolkit. Regulon activity was quantified as the area under the
831 curve (AUC) value and evaluated with the AUCell module. Active regulons were
832 defined based on the module's default AUC threshold. Differential regulon activity
833 across cell groups was assessed using the Wilcoxon rank-sum test via the
834 FindAllMarkers function in Seurat, with the following settings: logfc.threshold =0.25,
835 min.pct =0.1, pseudocount.use=FALSE, and only.pos =TRUE. Finally, a heatmap was
836 generated to display the z-score scaled regulon activity across identified cell clusters.

837 **3. Plasma Sample Detection Using Human Cytokine Array Q2000**

838 Plasma levels of 120 cytokines were measured with the Human Cytokine Array
839 QAH-CAA-2000 (RayBiotech). EDTA-anticoagulated plasma from Acute-infection
840 and normal groups (n=3 each) was centrifuged, aliquoted, and stored at −80°C. After
841 thawing and clarification, samples were diluted 2-fold with kit diluent. Array chips were
842 blocked, loaded with diluted plasma, and incubated overnight at 4°C. Following washes,
843 detection antibody cocktail and Cy3-streptavidin were applied sequentially.
844 Fluorescence was scanned (InnoScan 300, 532 nm) and analyte concentrations were
845 derived from standard curves ($R^2 \geq 0.95$; generated using serially diluted calibrators)
846 using the manufacturer's software, with sample concentrations interpolated based on
847 their fluorescence signals.

848 **4. Determination of plasm CXCL10 concentration using Dayou ELISA Kit**

849 CXCL10 concentration was determined using the Dayou precoated ELISA kit (Cat. No.
850 1117452). Plasma samples were pretreated with anticoagulant, centrifuged, and the
851 supernatant collected. All reagents were equilibrated to room temperature. A standard
852 curve was prepared by serial dilution (200 - 3.13 pg/mL). After adding standards, blank,

and samples to the plate, incubation and washing steps were performed sequentially with biotinylated antibody and streptavidin-HRP. TMB substrate was added for color development, followed by stop solution. Absorbance was measured at 450 nm within 10 min. Sample concentrations were interpolated from a four-parameter logistic (4-PL) standard curve ($R^2 > 0.95$), and all assays were performed with three technical replicates across two independent experiments.

5. RT-qPCR assay

Total RNA was extracted from plasma samples with TRIzol™ LS Reagent (Invitrogen, #10296010CN), and cDNA was synthesized (Vazyme, #R232) following the manufacturers' protocols. Quantitative real-time PCR was performed with SYBR Green (Vazyme, #Q412) in a 20 μL reaction volume. The cycling conditions comprised an initial denaturation step at 95 °C for 5 min, 45 cycles of 95 °C for 10 s and 60 °C for 30 s, and a subsequent melting curve analysis. Specifically, the forward primer of TAP1 was 5'-TGCCCCGCATATTCTCCCT-3' and the reverse primer was 5'-CACCTGCGTTTTCGCTCTTG-3'; for ISG15, the forward primer was 5'-CGCAGATCACCCAGAAGATCG-3' and the reverse primer was 5'-TTCGTCGCATTTGTCCACCA-3'; for GBP4, the forward primer was 5'-ATGGGTGAGAGAACTCTTCACG-3' and the reverse primer was 5'-TGCGGTATAGCCCTACAATGG-3'; for CMPK2, the forward primer was 5'-GTACCTCCTTTATTCCTGAAGCC-3' and the reverse primer was 5'-ATGGCAACAACCTGGAACTTT-3'; for OTOF, the forward primer was 5'-CAACAAGCGTGTCGCCTATG -3' and the reverse primer was 5'-TCCTTGCGCTGTTTGCTGA-3'; for SIGLEC1, the forward primer was 5'-CCTCGGGGAGGAACATCCTT-3' and the reverse primer was 5'-AGGCGTACCCCATCCTTGA-3'.

6. Evolutionary and mutational analyses

For raw FASTQ-format sequencing data, we first aligned reads to the human rRNA database using Bowtie2 (v2.4.5) and removed the aligned reads. We then used fastp

(v0.23.2) to filter out low-quality reads according to three criteria, including adapter contamination, the presence of uncertain nucleotides (N) in excess of 10% within a single read, and low-quality nucleotides (quality value < 20) accounting for more than 50% of a read. These high-quality reads were subsequently aligned to the human genome (GRCh38) via Bowtie2, while unaligned reads were aligned to the chikungunya virus genome (NC_004162.2). The BAM files generated from these alignments were processed with featureCounts (v2.0.1) for gene quantification. For virus-aligned BAM files, consensus sequence assembly was performed using the samtools (v1.15.1) mpileup command, and base mutations were analyzed with the iVar variants command. Finally, phylogenetic relationships among multiple viral strains (NC_004162.2, HM045816.1, HM045817.1, KP003809.1, MH229986.1, FJ445428.2, KX262989.1, JQ861258.1, MF076573.1, MH000703.1, MTO38402.1, HM045806.1, KX262990.1, MT591084.1, OK316994.1, KY435463.1, KR046234.1, MT666071.1, MT636912.1, Shenzhen/202507, Shenzhen/202508) were inferred using the Nextstrain bioinformatics pipeline. Briefly, genome sequences were aligned via MAFFT, and a maximum-likelihood phylogenetic tree was constructed using the tree module of Augur (v32.1.0). The resulting tree was further refined via temporal reconstruction and ancestral state inference with the Augur refine module, viral mutations were inferred using the Augur ancestral module, and the corresponding time-resolved phylogenetic tree was visualized with Auspice (https://auspice.us). After phylogenetic analysis with the Nextstrain pipeline, we selected MT666071.1 - the strain most closely related to our target CHIKV - as a new reference genome to enhance alignment accuracy. All sequencing reads were re-aligned to this optimized reference genome via Bowtie2, and subsequent variant calling was conducted using a custom pipeline integrating the samtools mpileup (v1.15.1) and iVar variants (v1.3.1) commands.

Acknowledgements

We gratefully acknowledge partial support for this work from the Biosafety Level III Laboratory and Biological Sample Bank of Shenzhen Third People's Hospital for bio-

samples and services, and the Center for Computational Science and Engineering at Southern University of Science and Technology. We thank all volunteers for their contributions to this research. The graphical abstract, Figure 1a and Figure 8 were created using BioRender (https://BioRender.com).

Author contributions

HY, ZY, RD, MZ, XL, JS and HL developed the concept of the project and wrote the paper. HY, ZY, SY and RD performed the experiments. XW, FO, XL, SH, YL, WL, TA, JY and XL analyzed the data with HY, HL and ZY. HY, MZ, TA, and HL supervised the project. All authors have read and agreed to the published version of the manuscript.

Funding

This work was supported by grants from the National Natural Science Foundation of China (No. 32300659); Shenzhen Science and Technology Innovation Commission Project (No. JCYJ20230807143302004); Shenzhen Clinical Research Center for Emerging Infectious Diseases (No. LCYSSQ20220823091203007); Guangdong Province Science and Technology Plan Project “Biosafety Technology” Special Project (No. 2022B111010003); Shenzhen High-level Hospital Construction Fund (No. XKJS-2025014, 23274G1001).

References

1 Bartholomeeusen, K. *et al.* Chikungunya fever. *Nat Rev Dis Primers* **9**, 17 (2023). https://doi.org:10.1038/s41572-023-00429-2

2 Ribeiro Dos Santos, G. *et al.* Global burden of chikungunya virus infections and the potential benefit of vaccination campaigns. *Nat Med* **31**, 2342-2349 (2025). https://doi.org:10.1038/s41591-025-03703-w

3 Wang, J. & Zhang, L. The chikungunya virus outbreak in Foshan, China: A rising public health threat in tropical and subtropical regions. *J Infect* **91**, 106591 (2025). https://doi.org:10.1016/j.jinf.2025.106591

4 Maure, C. *et al.* Chikungunya vaccine development, challenges, and pathway toward public health impact. *Vaccine* **42**, 126483 (2024). https://doi.org:10.1016/j.vaccine.2024.126483

5 Kolimenakis, A. *et al.* The role of urbanisation in the spread of Aedes mosquitoes and the diseases they transmit-A systematic review. *PLoS Negl Trop Dis* **15**, e0009631 (2021). https://doi.org:10.1371/journal.pntd.0009631

6 Tsetsarkin, K. A., Vanlandingham, D. L., McGee, C. E. & Higgs, S. A single mutation in chikungunya virus affects vector specificity and epidemic potential. *PLoS Pathog* **3**, e201 (2007). https://doi.org:10.1371/journal.ppat.0030201

7 Gloria-Soria, A. *et al.* Vector Competence of Aedes albopictus Populations from the Northeastern United States for Chikungunya, Dengue, and Zika Viruses. *Am J Trop Med Hyg* **104**, 1123-1130 (2020). https://doi.org:10.4269/ajtmh.20-0874

8 Ramphal, Y. *et al.* Understanding the Transmission Dynamics of the Chikungunya Virus in Africa. *Pathogens* **13** (2024). https://doi.org:10.3390/pathogens13070605

9 Tsetsarkin, K. A. & Weaver, S. C. Sequential adaptive mutations enhance efficient vector switching by Chikungunya virus and its epidemic emergence. *PLoS Pathog* **7**, e1002412 (2011). https://doi.org:10.1371/journal.ppat.1002412

10 Tsetsarkin, K. A. *et al.* Epistatic roles of E2 glycoprotein mutations in adaption of chikungunya virus to Aedes albopictus and Ae. aegypti mosquitoes. *PLoS One* **4**, e6835 (2009). https://doi.org:10.1371/journal.pone.0006835

11 Paixao, E. S. *et al.* Chikungunya chronic disease: a systematic review and meta-analysis. *Trans R Soc Trop Med Hyg* **112**, 301-316 (2018). https://doi.org:10.1093/trstmh/try063

12 Ren, J., Ling, F., Liu, Y. & Sun, J. Chikungunya in Zhejiang Province, Southeast China. *Infect Med (Beijing)* **2**, 315-323 (2023). https://doi.org:10.1016/j.imj.2023.11.005

13 Goncalves, W. A., de Sousa, C. D. F., Teixeira, M. M. & Souza, D. G. A brief overview of chikungunya-related pain. *Eur J Pharmacol* **994**, 177322 (2025). https://doi.org:10.1016/j.ejphar.2025.177322

14 Mapalagamage, M., Weiskopf, D., Sette, A. & De Silva, A. D. Current Understanding of the Role of T Cells in Chikungunya, Dengue and Zika Infections. *Viruses* **14** (2022). https://doi.org:10.3390/v14020242

15 Valdes-Lopez, J. F. *et al.* Interleukin 27, like interferons, activates JAK-STAT signaling and promotes pro-inflammatory and antiviral states that interfere with dengue and chikungunya viruses replication in human macrophages. *Front Immunol* **15**, 1385473 (2024). https://doi.org:10.3389/fimmu.2024.1385473

16 Roberts, G. C., Stonehouse, N. J. & Harris, M. The Chikungunya Virus nsP3 Macro Domain

Inhibits Activation of the NF-kappaB Pathway. *Viruses* **17** (2025). https://doi.org:10.3390/v17020191

17 Venugopalan, A., Ghorpade, R. P. & Chopra, A. Cytokines in acute chikungunya. *PLoS One* **9**, e111305 (2014). https://doi.org:10.1371/journal.pone.0111305

18 Kelvin, A. A. *et al.* Inflammatory cytokine expression is associated with chikungunya virus resolution and symptom severity. *PLoS Negl Trop Dis* **5**, e1279 (2011). https://doi.org:10.1371/journal.pntd.0001279

19 Sharma, S. K. & Jain, S. Chikungunya: A rheumatologist's perspective. *Int J Rheum Dis* **21**, 584-601 (2018). https://doi.org:10.1111/1756-185X.13273

20 Xiao, K. *et al.* A pan-immune panorama of bacterial pneumonia revealed by a large-scale single-cell transcriptome atlas. *Signal Transduct Target Ther* **10**, 5 (2025). https://doi.org:10.1038/s41392-024-02093-8

21 Bian, Z. *et al.* Deciphering human macrophage development at single-cell resolution. *Nature* **582**, 571-576 (2020). https://doi.org:10.1038/s41586-020-2316-7

22 Guilliams, M., Thierry, G. R., Bonnardel, J. & Bajenoff, M. Establishment and Maintenance of the Macrophage Niche. *Immunity* **52**, 434-451 (2020). https://doi.org:10.1016/j.immuni.2020.02.015

23 Ziegler-Heitbrock, L. *et al.* Nomenclature of monocytes and dendritic cells in blood. *Blood* **116**, e74-80 (2010). https://doi.org:10.1182/blood-2010-02-258558

24 Schilte, C. *et al.* Type I IFN controls chikungunya virus via its action on nonhematopoietic cells. *J Exp Med* **207**, 429-442 (2010). https://doi.org:10.1084/jem.20090851

25 Cook, L. E. *et al.* Distinct Roles of Interferon Alpha and Beta in Controlling Chikungunya Virus Replication and Modulating Neutrophil-Mediated Inflammation. *J Virol* **94** (2019). https://doi.org:10.1128/JVI.00841-19

26 Raftery, N. & Stevenson, N. J. Advances in anti-viral immune defence: revealing the importance of the IFN JAK/STAT pathway. *Cell Mol Life Sci* **74**, 2525-2535 (2017). https://doi.org:10.1007/s00018-017-2520-2

27 Gardner, J. *et al.* Chikungunya virus arthritis in adult wild-type mice. *J Virol* **84**, 8021-8032 (2010). https://doi.org:10.1128/JVI.02603-09

28 Blazquez-Moreno, A. *et al.* Transmembrane features governing Fc receptor CD16A assembly with CD16A signaling adaptor molecules. *Proc Natl Acad Sci U S A* **114**, E5645-E5654 (2017). https://doi.org:10.1073/pnas.1706483114

29 Ivetic, A., Hoskins Green, H. L. & Hart, S. J. L-selectin: A Major Regulator of Leukocyte Adhesion, Migration and Signaling. *Front Immunol* **10**, 1068 (2019). https://doi.org:10.3389/fimmu.2019.01068

30 Dunlock, V. E. Tetraspanin CD53: an overlooked regulator of immune cell function. *Med Microbiol Immunol* **209**, 545-552 (2020). https://doi.org:10.1007/s00430-020-00677-z

31 Simmons, D. P. *et al.* SLAMF7 engagement superactivates macrophages in acute and chronic inflammation. *Sci Immunol* **7**, eabf2846 (2022). https://doi.org:10.1126/sciimmunol.abf2846

32 Wu, Y. *et al.* SLAMF7 regulates the inflammatory response in macrophages during polymicrobial sepsis. *J Clin Invest* **133** (2023). https://doi.org:10.1172/JCI150224

33 Digiacomo, G., Ziche, M., Dello Sbarba, P., Donnini, S. & Rovida, E. Prostaglandin E2 transactivates the colony-stimulating factor-1 receptor and synergizes with colony-stimulating factor-1 in the induction of macrophage migration via the mitogen-activated protein kinase

ERK1/2. *FASEB J* **29**, 2545-2554 (2015). https://doi.org:10.1096/fj.14-258939

34 Guma, M., Ronacher, L. M., Firestein, G. S., Karin, M. & Corr, M. JNK-1 deficiency limits macrophage-mediated antigen-induced arthritis. *Arthritis Rheum* **63**, 1603-1612 (2011). https://doi.org:10.1002/art.30271

35 Sha, H., Zhang, D., Zhang, Y., Wen, Y. & Wang, Y. ATF3 promotes migration and M1/M2 polarization of macrophages by activating tenascin-C via Wnt/beta-catenin pathway. *Mol Med Rep* **16**, 3641-3647 (2017). https://doi.org:10.3892/mmr.2017.6992

36 Long, K. M. & Heise, M. T. Protective and Pathogenic Responses to Chikungunya Virus Infection. *Curr Trop Med Rep* **2**, 13-21 (2015). https://doi.org:10.1007/s40475-015-0037-z

37 Brandstadter, J. D. & Yang, Y. Natural killer cell responses to viral infection. *J Innate Immun* **3**, 274-279 (2011). https://doi.org:10.1159/000324176

38 Petitdemange, C. *et al.* Unconventional repertoire profile is imprinted during acute chikungunya infection for natural killer cells polarization toward cytotoxicity. *PLoS Pathog* **7**, e1002268 (2011). https://doi.org:10.1371/journal.ppat.1002268

39 Borgherini, G. *et al.* Outbreak of chikungunya on Reunion Island: early clinical and laboratory features in 157 adult patients. *Clin Infect Dis* **44**, 1401-1407 (2007). https://doi.org:10.1086/517537

40 Karin, N. CXCR3 Ligands in Cancer and Autoimmunity, Chemoattraction of Effector T Cells, and Beyond. *Front Immunol* **11**, 976 (2020). https://doi.org:10.3389/fimmu.2020.00976

41 Yan, Q. *et al.* CC chemokines Modulate Immune responses in Pulmonary Hypertension. *J Adv Res* **63**, 171-186 (2024). https://doi.org:10.1016/j.jare.2023.10.015

42 Adams, R. C., MacDonald, K. P. A. & Hill, G. R. The contribution of the monocyte-macrophage lineage to immunotherapy outcomes. *Blood* **145**, 1010-1021 (2025). https://doi.org:10.1182/blood.2024025680

43 Rulli, N. E. *et al.* Protection from arthritis and myositis in a mouse model of acute chikungunya virus disease by bindarit, an inhibitor of monocyte chemotactic protein-1 synthesis. *J Infect Dis* **204**, 1026-1030 (2011). https://doi.org:10.1093/infdis/jir470

44 Elemam, N. M., Talaat, I. M. & Maghazachi, A. A. CXCL10 Chemokine: A Critical Player in RNA and DNA Viral Infections. *Viruses* **14** (2022). https://doi.org:10.3390/v14112445

45 Zheng, Q. *et al.* Siglec1 suppresses antiviral innate immune response by inducing TBK1 degradation via the ubiquitin ligase TRIM27. *Cell Res* **25**, 1121-1136 (2015). https://doi.org:10.1038/cr.2015.108

46 Michalski, N. *et al.* Otoferlin acts as a Ca(2+) sensor for vesicle fusion and vesicle pool replenishment at auditory hair cell ribbon synapses. *Elife* **6** (2017). https://doi.org:10.7554/eLife.31013

47 Wilson, J. A. *et al.* RNA-Seq analysis of chikungunya virus infection and identification of granzyme A as a major promoter of arthritic inflammation. *PLoS Pathog* **13**, e1006155 (2017). https://doi.org:10.1371/journal.ppat.1006155

48 Bae, S., Lee, J. Y. & Myoung, J. Chikungunya Virus nsP2 Impairs MDA5/RIG-I-Mediated Induction of NF-kappaB Promoter Activation: A Potential Target for Virus-Specific Therapeutics. *J Microbiol Biotechnol* **30**, 1801-1809 (2020). https://doi.org:10.4014/jmb.2012.12005

49 Davenport, B. J. *et al.* Chikungunya Virus Evades Antiviral CD8(+) T Cell Responses To Establish Persistent Infection in Joint-Associated Tissues. *J Virol* **94** (2020). https://doi.org:10.1128/JVI.02036-19

50 Wauquier, N. *et al.* The acute phase of Chikungunya virus infection in humans is associated with strong innate immunity and T CD8 cell activation. *J Infect Dis* **204**, 115-123 (2011). https://doi.org:10.1093/infdis/jiq006

51 Lin, T. *et al.* CXCL10 Signaling Contributes to the Pathogenesis of Arthritogenic Alphaviruses. *Viruses* **12** (2020). https://doi.org:10.3390/v12111252

52 Lane, B. R. *et al.* The C-X-C chemokine IP-10 stimulates HIV-1 replication. *Virology* **307**, 122-134 (2003). https://doi.org:10.1016/s0042-6822(02)00045-4

53 Zhao, T., Chen, T., Zhang, J., Li, C. & Qin, C. Chikungunya virus: Current situation and future challenges. *Biosaf Health* **7**, 348-356 (2025). https://doi.org:10.1016/j.bsheal.2025.10.001

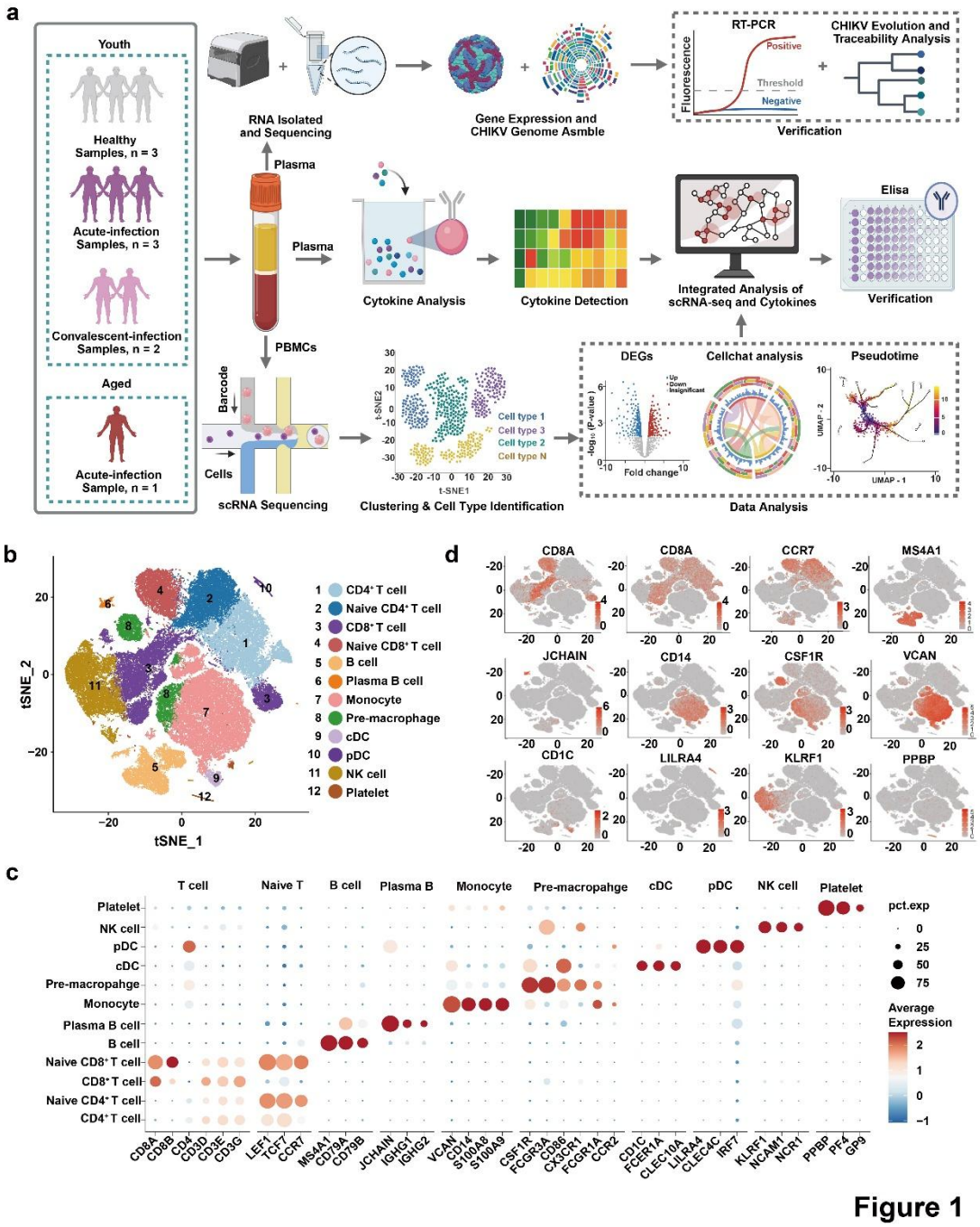

Figure 1

Figure 1. Identification of cell populations among the PBMCs by scRNA-seq. a Schematic overview of the study design and experimental workflow. **b** t-SNE visualization of all PBMC-derived cells from all cohorts, annotated to 12 major cell types. **c** Expression levels of selected canonical cell markers in 12 major cell types, with the color and size of each point corresponding to the cellular expression fraction of the marker genes, respectively. **d** t-SNE projections illustrating the expression patterns of representative canonical marker genes for each cell type. In each panel,

color intensity reflects the expression level of the indicated gene (darker shades = higher expression).

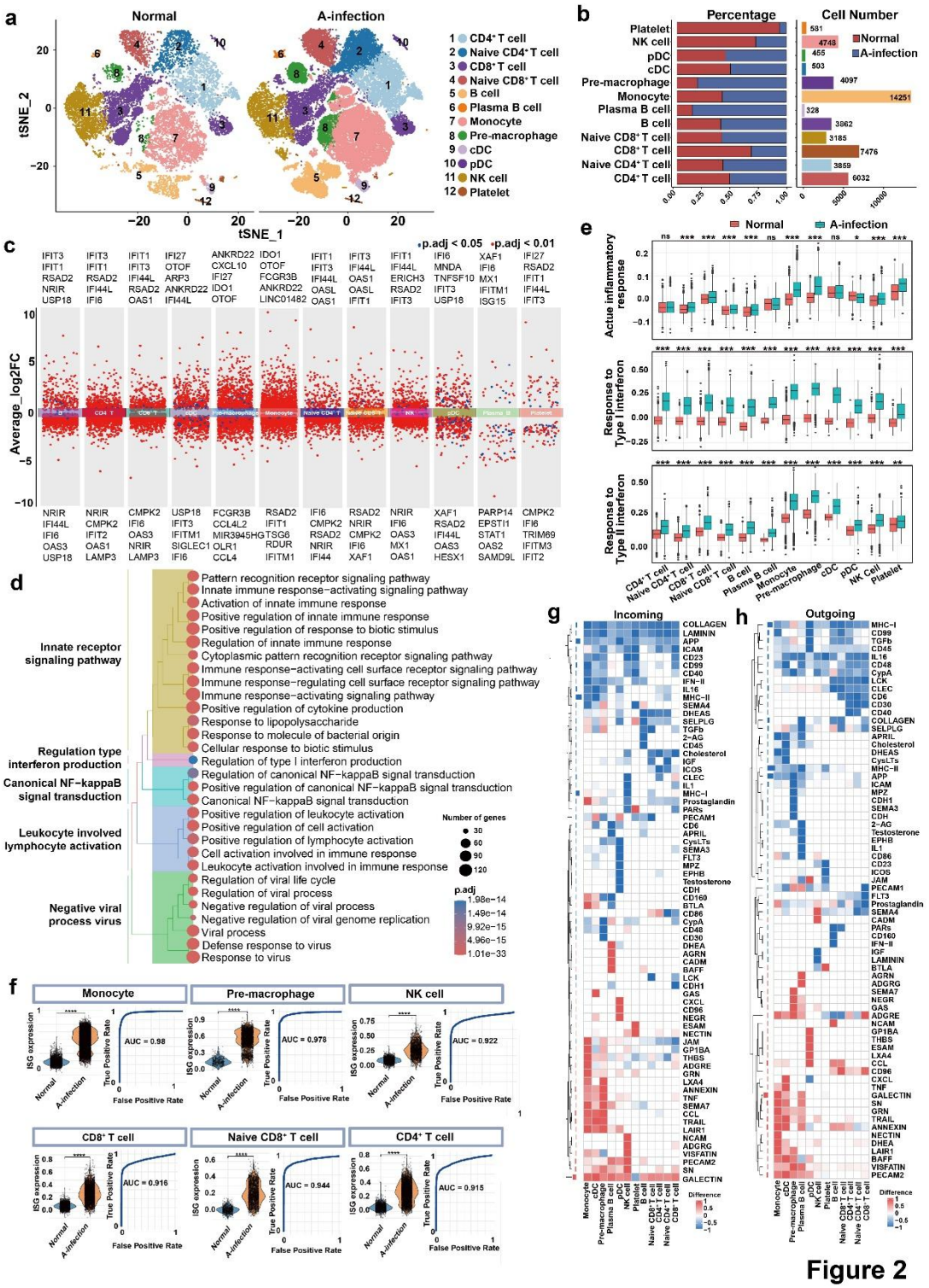

Figure 2

Figure 2. Differential cellular clustering and molecular response profiling between CHIKV A-infection and normal cohorts. a t-SNE visualization of cellular cluster composition in normal vs. A-infection groups. **b** Dual-panel bar chart depicting the abundance of distinct cell types: the left panel illustrates the proportional abundance of each cell cluster, while the right panel presents the corresponding absolute cell numbers. **c** Combined volcano plots identifying DEGs for each cell type

(A-infection vs. normal), the top five ranked genes are listed for each cluster. **d** Hierarchical tree plot of GO enrichment analysis for up-regulated DEGs. **e** Box plots illustrating expression patterns of representative GO terms across all cell types (A-infection vs. normal). **f** (left) Violin plot illustrating the activation levels of ISG-related genes across all cell types in A-infection versus normal groups; (right) Receiver operating characteristic (ROC) curves, with corresponding AUC values indicated, evaluating the diagnostic potential of ISG-related genes. **g-h** Heatmap showing differences in intercellular signaling across distinct cell types between the A-infection group and the normal group: (left) Differences in incoming signaling; (right) Differences in outgoing signaling. Red indicates elevated signal intensity in the A-infection group compared with the normal group, while blue indicates reduced signal intensity; deeper color represents greater magnitude of signal change. Statistical significance was analyzed by Wilcoxon rank-sum test, ns = not significant, *P < 0.05, **P < 0.01, ***P < 0.001.

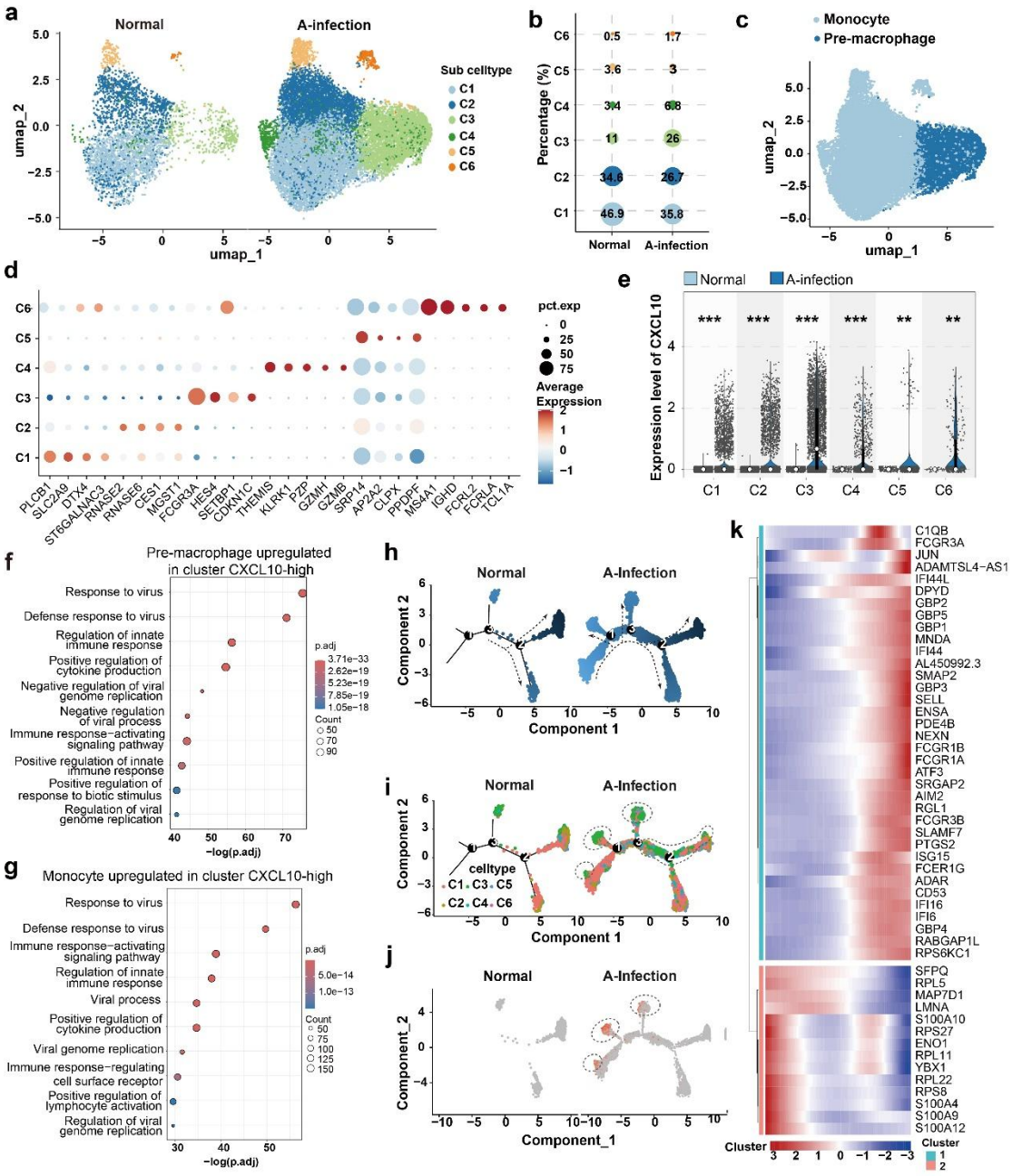

Figure 3

Figure 3. Dissection of cellular heterogeneity in monocyte and pre-macrophage lineage cells. **a** UMAP visualization of 6 subclusters (C1-C6) from monocyte and pre-macrophage populations, displayed for normal and A-infection groups separately. **b** Bubble plot of subcluster percentage composition in normal and A-infection groups. **c** UMAP plot showing the distribution of monocytes and pre-macrophages: monocytes (light blue) and pre-macrophages (dark blue). **d** Dot plot of highly expressed genes in each subclusters. **e** Violin plots of CXCL10 expression across subclusters. **f-g** GO enrichment showing the significantly enriched terms in CXCL10-highly expressed pre-macrophages and monocytes; (**f**) Significantly enriched biological processes in CXCL10-highly

expressed pre-macrophages, (**g**) Significantly enriched biological processes in CXCL10-highly expressed monocytes. **h** The root node selection for monocyte and pre-macrophage lineages of pseudotime trajectory, dashed line represents the pseudotime trajectory. **i** Pseudotime trajectory plot showing the developmental trajectory of subclusters, the dashed circle denotes the region where Subcluster C3 is relatively concentrated. **j** Pseudotime trajectory plot showing the distribution of CXCL10-highly expressed subclusters. **k** Heatmap showing genes highly expressed at the initial and terminal stages of pseudotime development. blue = low, red = high expression.

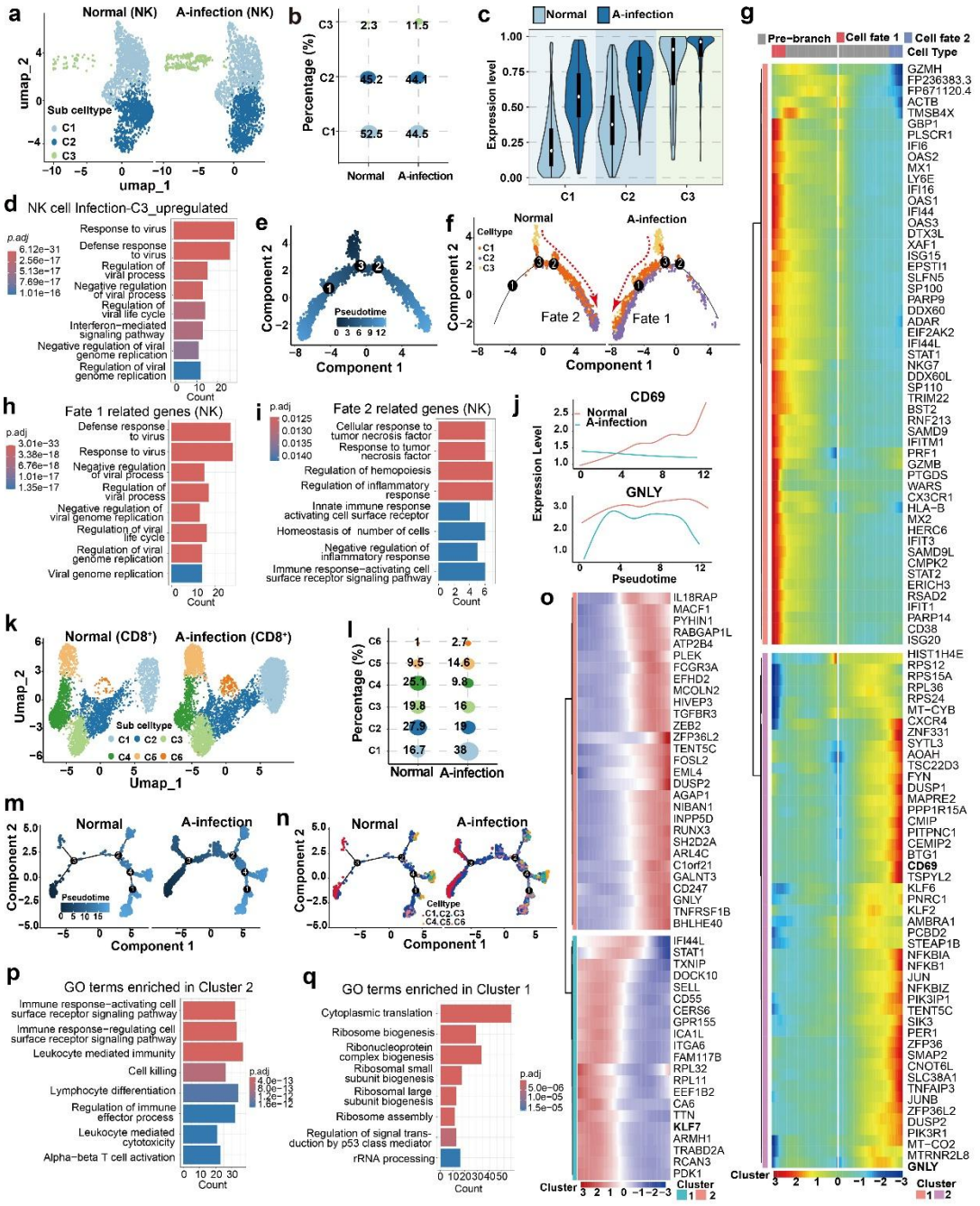

Figure 4

Figure 4. Subclustering and immunological characterization of NK cells and CD8⁺ T cells. a UMAP visualization of NK cells, colored by 3 distinct subclusters (C1-C3). **b** Proportional abundance of each NK cell subcluster in A-infection and normal groups. **c** Differentiation potential of the three NK subclusters as predicted by CytoTRACE analysis. **d** Significantly enriched GO terms in the C3 subcluster. **e** Pseudotime trajectory analysis reconstructing the developmental continuum of NK cells. **f** Pseudotime trajectory plot depicting fate divergence of NK subclusters in A-infection vs. normal groups. **g** Heatmap comparing gene expression patterns between two

terminal cellular fates (Fate1 and Fate2). **h-i** Bar plots displaying the significantly enriched GO terms associated with Fate1 (h) and Fate2 (i). **j** Expression dynamics of CD69 and GNLY along reconstructed pseudotime in A-infection vs. normal NK cells. **k** UMAP visualization of $CD8^+$ T cells, annotated by six distinct subclusters (C1-C6). **l** Stacked bar plot showing proportional changes of each $CD8^+$ T cell subcluster in A-infection vs. normal groups. **m** Pseudotime trajectory analysis reconstructing the developmental continuum of $CD8^+$ T cells. **n** Pseudotime trajectory plot depicting fate divergence of $CD8^+$ T cell subclusters (C1-C6) in A-infection vs. normal groups. **o** Heatmap showing genes highly expressed at the initial and terminal stages of pseudotime development. **p-q** Bar plots displaying significantly enriched GO terms associated with Cluster 2 (**p**) and Cluster 1 (**q**) in chart **o**.

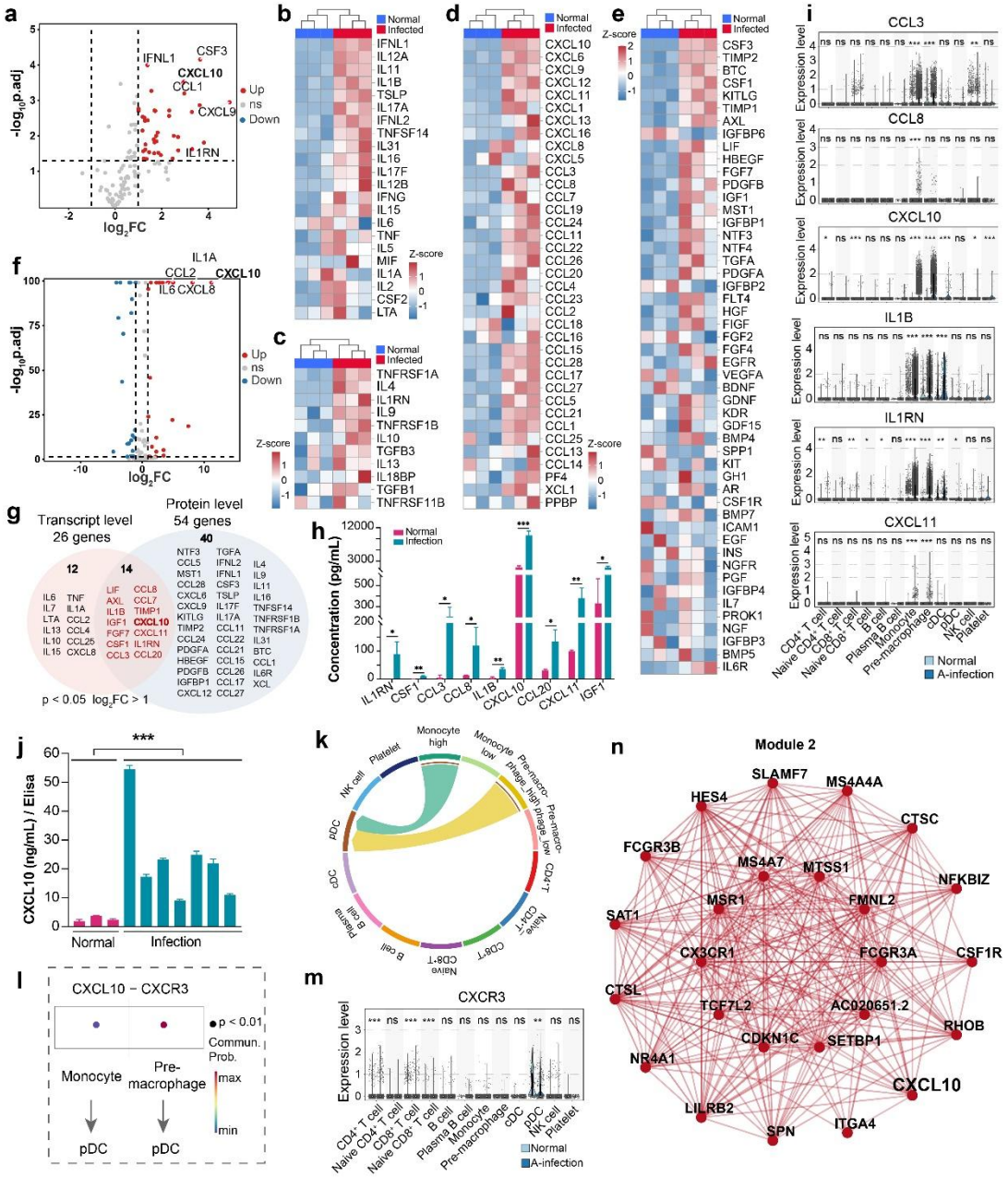

Figure 5

Figure 5. Integrated analysis of plasma cytokine array and scRNA-seq. a Volcano plot showing differential expression analysis of 120 immune-related genes from plasma protein array data, with cutoff criteria of $log_2FC > 1$ and $p < 0.05$. Red dots: significantly upregulated immune factors in infected patients; blue dots: significantly downregulated ones; gray dots: no significant alteration. **b-e** Heatmaps displaying 120 plasma factors stratified into four functional categories: (**b**) pro-inflammatory cytokines, (**c**) anti-inflammatory cytokines, (**d**) chemokines, and (**e**) growth factors; color scale represents z-score-normalized expression. **f** Volcano plot showing the differential

expression analysis of 120 immune factor-related gene transcripts from scRNA-seq data of all PBMCs (A-infection vs. Normal, $log_2FC > 1$ and $p < 0.05$). Red dots: significantly upregulated immune factors in infected patients; blue dots: significantly downregulated ones; gray dots: no significant alteration. **g** Venn diagram illustrating the 14-gene overlapping set between differentially expressed proteins (plasma array) and transcripts (scRNA-seq), defined by $log_2FC > 1$ and $p < 0.05$. **h** Bar plot showing the fold change of the top 10 upregulated overlapping genes between plasma proteins and scRNA-seq transcripts. **i** Violin plot illustrating the expression patterns of key cytokines from the 14 overlapping hits (CCL3, CCL8, CXCL10, IL1RN, IL1B, CXCL11) that were significantly upregulated in monocytes and macrophages. **j** Bar plot of plasma CXCL10 concentration (pg/mL) in infected cohorts vs. Normal, quantified by Elisa. **k** Chord diagram of the CXCL signaling pathway network, where segments denote distinct immune cell types and chords indicate intercellular interactions. CXCL10-highly expressed monocytes and macrophages were isolated. **l** Ligand-receptor interaction analysis of CXCL10-CXCR3, p-value denotes interaction significance. **m** Violin plots depicting CXCR3 expression levels across distinct immune cell subsets in Normal vs. A-infection cohorts. **n** WGCNA co-expression network of module M2, where red nodes represent genes and red edges denote significant co-expression relationships. Statistical significance was determined by the Wilcoxon rank-sum test: $*P < 0.05$, $**P < 0.01$, $***P < 0.001$.

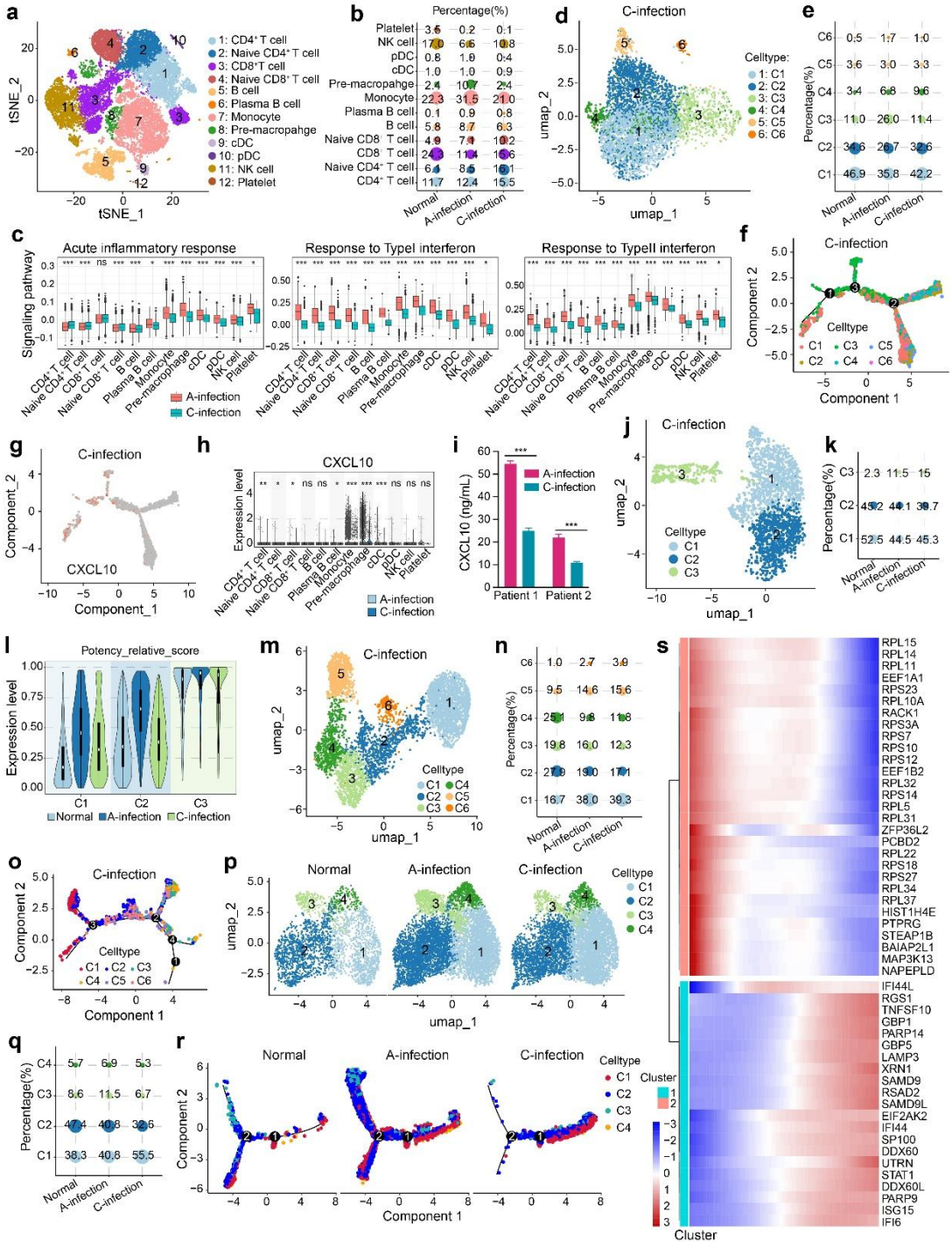

Figure 6

Figure 6. Analysis of stage-specific immunokinetics in patients during the convalescent phase of CHIKV infection. a t-SNE plot showing cellular cluster composition in Normal, A-infection, and C-infection groups. **b** Bubble plot illustrating percentage distribution of 12 immune cell types across three groups. **c** Box plots of transcriptional responses (acute inflammatory response, Type I interferon and Type II interferon responses) across distinct cell types between A-infection and C-

infection groups. **d** UMAP plot displaying subclustering of monocytes and pre-macrophages in the C-infection group. **e** Bubble plot illustrating percentage distribution of monocyte and pre-macrophage subpopulations across three groups. **f** Pseudotime trajectory plot depicting differentiation dynamics of monocyte and pre-macrophage subpopulations in the C-infection group. **g** Pseudotime trajectory plot illustrating CXCL10 expression dynamics across monocyte and pre-macrophage subpopulations in the C-infection group. **h** Violin plot showing CXCL10 expression levels in PBMSs from A-infection and C-infection groups. **i** Bar plot of plasma CXCL10 concentration (pg/mL) in A-infection vs. C-infection patients, quantified by ELISA. **j** UMAP plot displaying subclustering of NK cells in the C-infection group. **k** Bubble plot illustrating percentage distribution of NK cell subpopulations across Normal, A-infection, and C-infection groups; **l** Violin plot depicting Potency relative score expression levels across NK cell subpopulations across three groups. **m** UMAP plot displaying subclustering of $CD8^+$ T cells in the C-infection group. **n** Bubble plot illustrating percentage distribution of $CD8^+$ T cell subpopulations across three groups. **o** Pseudotime trajectory plot depicting differentiation dynamics of $CD8^+$ T cell subpopulations in the C-infection group. **p** UMAP plots showing $CD4^+$ T cell distribution across three groups. **q** Bubble plot illustrating percentage distribution of $CD4^+$ T cell subpopulations across three groups. **r** Pseudotime trajectory plots showing differentiation dynamics of $CD4^+$ T cell subpopulations across three groups. **s** Heatmap showing genes highly expressed at the initial and terminal stages of pseudotime development ($CD4^+$). Statistical significance was analyzed by Wilcoxon rank-sum test, $^*P < 0.05$, $^{**}P < 0.01$, $^{***}P < 0.001$.

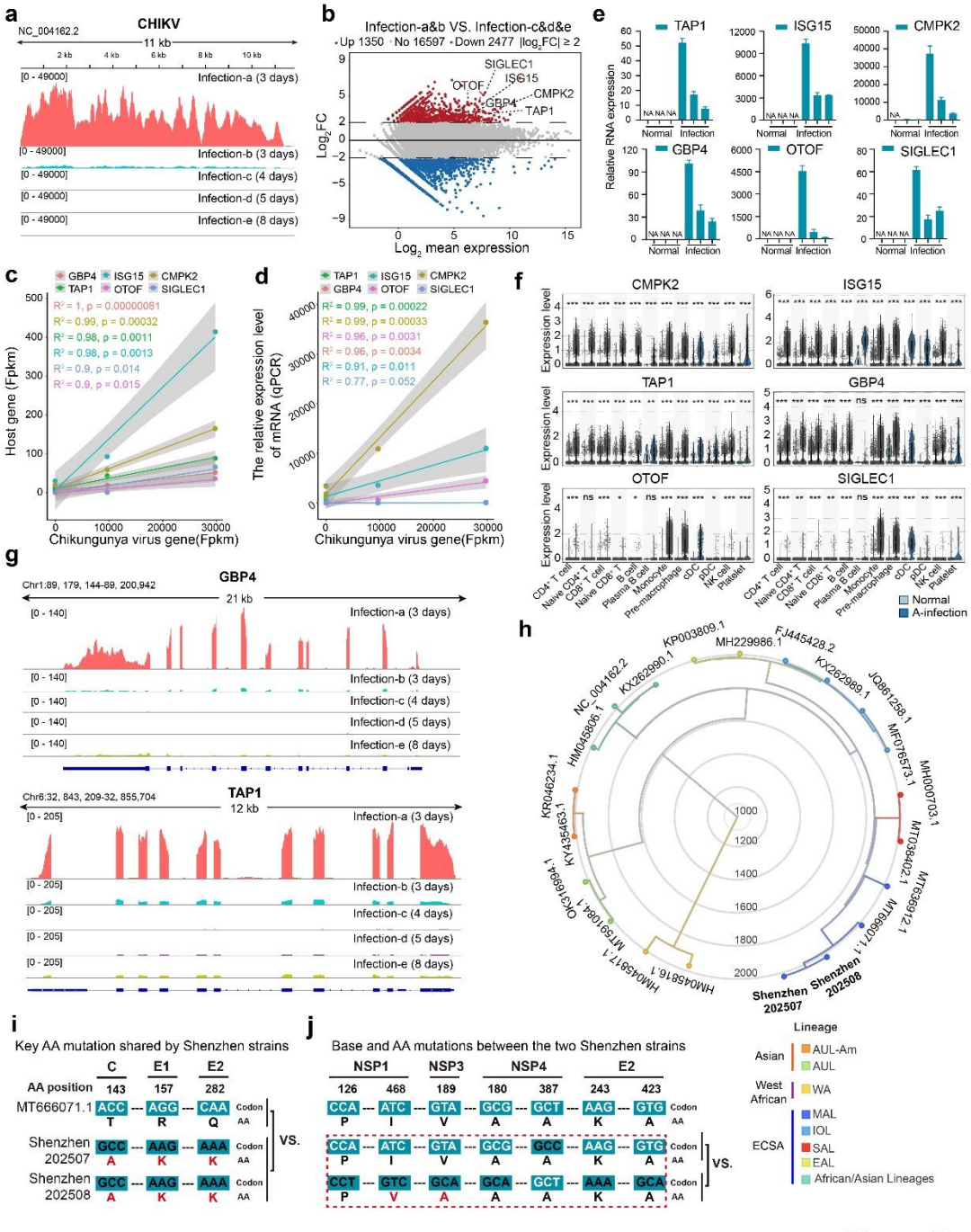

Figure 7

Figure 7. CHIKV lineage analysis and identification of plasma biomarkers. a IGV plot of CHIKV normalized read counts in plasma. Infection-a (sample ID: P1), Infection-b (sample ID: P2), Infection-c (sample ID: P3), Infection-d (sample ID: P4), Infection-e (sample ID: P5). **b** MA plot highlighting DEGs (|log2FC| ≥ 2) between infection a & b and infection c & d & e. Red: upregulated genes; blue: downregulated genes; gray: non-significant. Dashed lines indicate significance thresholds. **c** Correlation plot of FPKM values between host mRNA and viral genome in plasma. **d**

Correlation plot of qPCR relative quantification values of host mRNA and FPKM values of viral genome in plasma. **e** qPCR results showing the relative expression levels of relevant mRNAs in plasma from the normal group and infected group. The ID of the three infected patients: P1, P2, P3. **f** Violin plot showing the TAP1, ISG15, CMPK2, GBP4, OTOF, and SIGLEC1 expression levels in PBMCs from A-infection and normal group. **g** IGV plot showing normalized read counts of GBP4 and TAP1 genes in plasma. **h** Radial plot of phylogenetic relationships between multiple strains. AUL-Am: Asian Urban + American Lineage, AUL: Asian Urban Lineage, WA: Western African Lineage, MAL: Middle African Lineage, IOL: Indian Ocean Lineage, SAL: South American Lineage, EAL: Eastern African Lineage. **i** Shared amino acid mutations in the structural protein regions between the two Shenzhen viral strains compared with MT666071.1. **j** Nucleotide and amino acid mutations in the structural and non-structural protein regions between the two Shenzhen CHIKV strains. AA: amino acid.

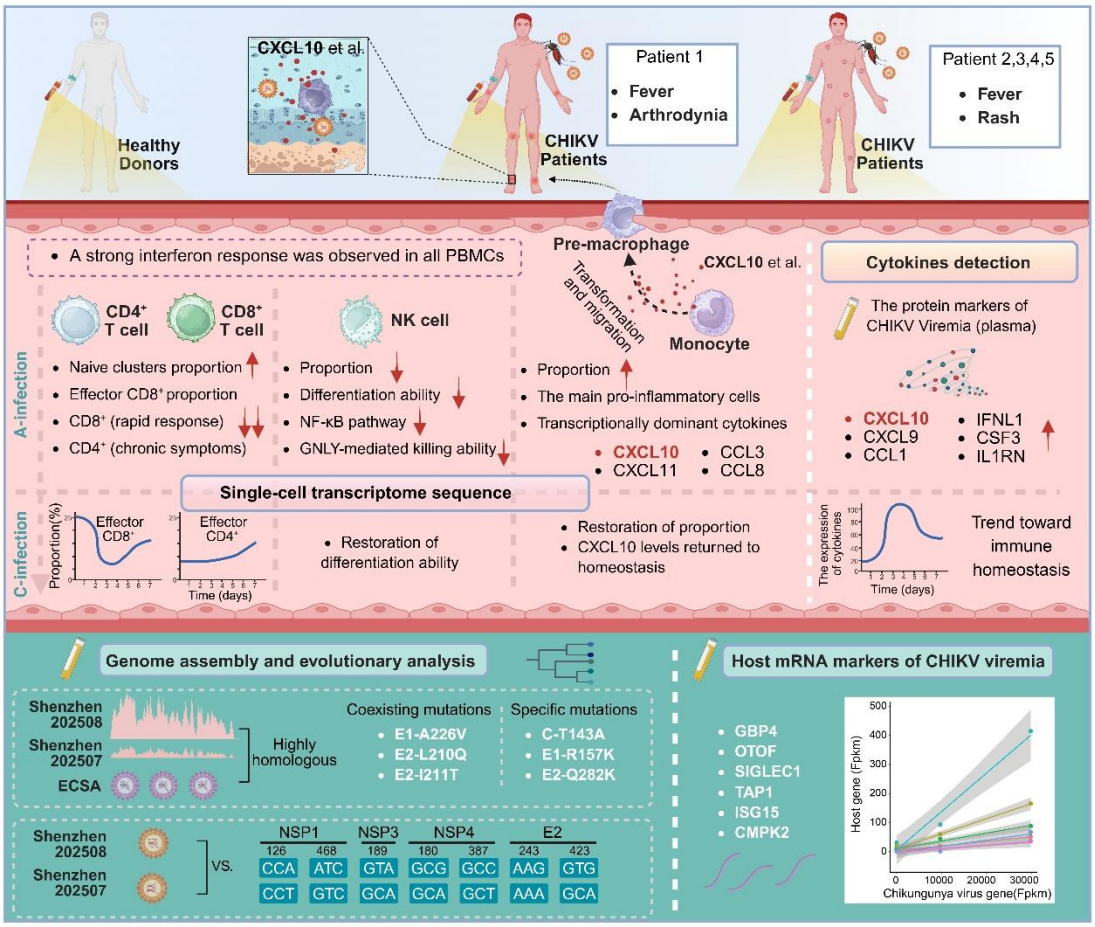

Figure 8. Summary of the experimental hierarchical design and key findings of the entire study.

Table 1. Characteristics and laboratory findings of healthy donors and enrolled patients infected with Chikungunya virus in the study.

	Normal			Infection				
Sample ID	N1	N2	N3	P1	P2	P3	P4	P5
Charateristics								
Age, years	36	26	24	16	19	23	57	34
Sex	Male	Female	Female	Female	Male	Female	Female	Male
Time[#]	N/A	N/A	N/A	3d/7d	3d	4d/6d	5d	8d
Fever	No	No	No	Yes	Yes	Yes	Yes	Yes
Rash	No	No	No	No	Yes	Yes	Yes	Yes
Arthrodynia	No	No	No	Yes	No	No	No	No
Blood routine	Reference range							
Leucocytes count, × 10^9/L	3.5-9.5			5.34	3.73	3.71	4.17	3.69
Neutrophils count, × 10^9/L	1.8-6.3			4.25	2.48	1.50 ↓	2.80	2.14
Lymphocytes count, × 10^9/L	1.1-3.2			0.53 ↓	0.75 ↓	0.78 ↓	0.81 ↓	1.06 ↓
Platelets count, × 10^9/L	125-350			187	307	240	191	274
Haemoglobin, g/L	115-150			141	118	165 ↑	140	121
Blood biochemistry	Reference range							
Albumin, g/L	40-55			43.9	45.2	47.1	48.9	45.7
Alanine aminotransferase, U/L	0-40			19	7	10	33	11
Aspartate aminotransferase, U/L	0-35			30	18	20	21	17
Total bilirubin, μmol/L	0-21			11.7	14.5	10.1	11.9	8.9
C-reactive protein, mg/L	0-6			24.57 ↑	3.40	8.40 ↑	12.43 ↑	2.47
Interleukin-6, pg/mL	0-7			25.80 ↑	11.9 ↑	1.91	5.22	N/D

"#" refers to the interval from symptom onset to PBMCs collection. PBMCs from Patient 1 (P1) were collected at 3 and 7 days post symptom onset, while those from Patient 3 (P3) were collected at 4 and 6 days post symptom onset. N/A: Not applicable; N/D: Not detected.

In this study, peripheral blood samples were collected from 8 volunteers for subsequent data analysis, including 3 healthy controls and 5 infected patients (2 of whom were sampled at two separate time points). The samples used for the experiments are as follows. Single-cell transcriptome sequencing was performed on PBMCs isolated from 3 healthy controls, the primary samples of infected individuals P1-P5, and the secondary sample of infected individual P1. CXCL10 levels were quantified via ELISA in 7 plasma samples from the 5 infected patients (including samples at different time points) and 3 plasma samples from healthy controls. Plasma sequencing was conducted using primary plasma samples of the 5 infected individuals. Data for cytokine and qPCR assays were obtained from the primary plasma samples of infected patients P1, P2 and P3.